



**HAL**  
open science

## **NiCo<sub>2</sub>O<sub>4</sub> nanostructures loaded onto pencil graphite rod: An advanced composite material for oxygen evolution reaction**

Zafar Hussain Ibupoto, Aneela Tahira, Aqeel Ahmed Shah, Umair Aftab, Muhammad Yameen Solangi, Jaleel Ahmed Leghari, Abdul Hanan Samoon, Adeel Liaquat Bhatti, Muhammad Ali Bhatti, Raffaello Mazzaro, et al.

### ► To cite this version:

Zafar Hussain Ibupoto, Aneela Tahira, Aqeel Ahmed Shah, Umair Aftab, Muhammad Yameen Solangi, et al.. NiCo<sub>2</sub>O<sub>4</sub> nanostructures loaded onto pencil graphite rod: An advanced composite material for oxygen evolution reaction. *International Journal of Hydrogen Energy*, 2022, 47 (10), pp.6650-6665. 10.1016/j.ijhydene.2021.12.024 . hal-03519731

**HAL Id: hal-03519731**

**<https://hal.univ-lorraine.fr/hal-03519731>**

Submitted on 30 Sep 2022

**HAL** is a multi-disciplinary open access archive for the deposit and dissemination of scientific research documents, whether they are published or not. The documents may come from teaching and research institutions in France or abroad, or from public or private research centers.

L'archive ouverte pluridisciplinaire **HAL**, est destinée au dépôt et à la diffusion de documents scientifiques de niveau recherche, publiés ou non, émanant des établissements d'enseignement et de recherche français ou étrangers, des laboratoires publics ou privés.



Distributed under a Creative Commons Attribution 4.0 International License

## **NiCo<sub>2</sub>O<sub>4</sub> nanostructures loaded onto pencil graphite rod: An advanced composite material for oxygen evolution reaction**

Zafar Hussain Ibupoto<sup>a\*</sup>, Aneela Tahira<sup>a\*</sup>, Aqeel Ahmed Shah<sup>d</sup>, Umair Aftab<sup>b</sup>, Muhammad Yameen Solangi<sup>b</sup>, Jaleel Ahmed Leghari<sup>b</sup>, Abdul Hanan Samoon<sup>b</sup>, Adeel Liaquat Bhatti<sup>c</sup>, Muhammad Ali Bhatti<sup>c</sup>, Raffaello Mazzaro<sup>f</sup>, Vittorio Morandi<sup>f</sup>, Muhammad Ishaq Abro<sup>b</sup>, Ayman Nafady<sup>g</sup>, Abdullah M Al-Enizi<sup>g</sup>, Mélanie Emo<sup>i</sup>, Brigitte Vigolo<sup>i\*</sup>

<sup>a</sup>Dr. M.A Kazi Institute of Chemistry University of Sindh Jamshoro, 76080, Sindh Pakistan

<sup>b</sup>Mehran University of Engineering and Technology, 7680 Jamshoro, Sindh Pakistan

<sup>c</sup>Institute of Physics University of Sindh Jamshoro, 76080, Sindh Pakistan

<sup>d</sup>NED University of Engineering and Technology Karachi, Sindh Pakistan

<sup>e</sup>Department of Environmental Sciences University of Sindh Jamshoro, 76080, Sindh Pakistan

<sup>f</sup>Institute for Microelectronics and Microsystems, Italian National Research Council, Section of Bologna, Via Piero Gobetti 101, 40129, Bologna, Italy

<sup>g</sup>Department of Chemistry, College of Science, King Saud University, Riyadh 11451, Saudi Arabia

<sup>i</sup>Université de Lorraine, CNRS, IJL, F-54000 Nancy, France

Corresponding authors: Zafar Hussain Ibupoto, PhD\*, Brigitte Vigolo, PhD, Aneela Tahira, PhD

Email address: zaffar.ibhupoto@usindh.edu.pk, brigitte.vigolo@univ-lorraine.fr

[aneelatahira80@gmail.com](mailto:aneelatahira80@gmail.com)

### **Abstract**

Driving oxygen evolution reaction (OER) at extremely low overpotential and the blockage of oxygen gas inside the catalytic material leads to the deactivation of catalytic activity, therefore it is an essential step in electrochemical energy conversion systems, but still very challenging task. The clay minerals including bentonite and kaolinite are rich with plenty of active centers and favorable chemical composition for the catalysis applications but limited by the insulating properties, thus they cannot be used as an electrode material for the water splitting. The unique

presence of clay minerals in the form of pencil graphite rod (PGR) and its attractive architecture enabled us to exploit advantageous features and use them as an in situ electrode for growth of metal oxide nanostructures for the electrolysis applications. The naturally inherent presence of SiO<sub>2</sub> favors the catalytic properties and durability of the electrode whereas the MgO produces the abundant oxygen vacancies and Co<sup>3+</sup> ions for OER process. Herein, we present a facile approach of using PGR as host substrate and co-catalyst for the loading of Co<sub>3</sub>O<sub>4</sub>, NiCo<sub>2</sub>O<sub>4</sub> and NiO nanostructures and the modified electrode carried high porosity for easily bubbling of oxygen gas, plenty of intrinsic active centers coming from both clay minerals and metal oxides for excellent OER process. The fabricated electrode is physically well-characterized, and it has a natural ability to sustain a long term stability even at higher current densities and industrial electrolyzer conditions. The NiCo<sub>2</sub>O<sub>4</sub>/PGR, Co<sub>3</sub>O<sub>4</sub>/PGR, and NiO/PGR electrodes exhibit an overpotential of 234, 242 and 272 mV respectively at a current density of 100 mAcm<sup>-2</sup> in 1.0 M KOH electrolytic solution. The presence of large number of oxygen vacancies through SiO<sub>2</sub> and MgO, high Ni<sup>2+</sup>/Ni<sup>3+</sup> and Co<sup>3+</sup>/Co<sup>2+</sup> ratios, multi metal centers, large specific surface area, high pore volume, high electrochemical active surface area and fast charge transport within the NiCo<sub>2</sub>O<sub>4</sub>/PGR are the main reasons for its superfast OER kinetics. Thus, the proposed method of electrode design will pave a potential way for high performance electrochemical devices like metal air batteries, fuel cell and supercapacitors.

**Keywords:** Pencil graphite rod, Metal Oxides, MgO, SiO<sub>2</sub>, Oxygen Evolution Reaction

## 1. Introduction

Electrochemical water splitting is a route of great importance for the next generation of green energy. In the electrochemical energy conversion system, the oxygen evolution reaction (OER) is the main pillar which plays an important role in metal air batteries, photoelectrochemical cells, water splitting and fuel cell technologies [1-6]. OER is known as the limiting reaction in water electrolysis devices [7] due to the high overpotential required with most catalysts, resulting from the sluggish kinetics of the 4-electron reaction [8]. To date, precious metal-based catalysts (Ir, Ru, RuO<sub>2</sub> and IrO<sub>2</sub>) are the most efficient OER catalysts [9-12] but their scalability is not feasible. For a reliable and economically sustainable water electrolysis technology, it is urgently required to develop low overpotential catalysts. Improvements in the performance of OER catalysts depend critically on the success of work aimed at finding new routes and new materials to design precious metal-free electrocatalysts. The efforts towards this goal are mainly devoted to the development of efficient earth abundant-based catalysts, as well as to the optimization of the conductive supporting material, providing both high surface area and low charge transfer resistance to the catalyst. The transition metals of first row including (Mn, Fe, Co and Ni) have received lot of attention because of their earth abundance nature and theoretically high catalytic performance [13-17]. The spinel oxides composed of transition metals like Co [18-22], Ni [23,24], Zn [25], Mn [26,27], and Fe [28, 29] have been identified as potential electrocatalysts for OER application. Co<sub>3</sub>O<sub>4</sub> is one of the spinel oxides which was found to be an excellent OER electrocatalyst [30-33]. Beside this, bimetallic oxides of cobalt having a spinel structure were investigated in the wide range of energy storage and conversion applications [34-36]. Among them, nickel-cobalt bimetallic oxides of NiCo<sub>2</sub>O<sub>4</sub> have been intensively studied in different electrochemical applications in the recent past [37-43]. NiCo<sub>2</sub>O<sub>4</sub> is a nonprecious bimetallic oxide and it is highly active for various electrocatalysis applications such as OER, HER, ORR and alcohol oxidation reactions [44-49]. NiO was shown to exhibit a considerable catalytic activity in half-cell OER reaction [50]. However, the poor electrical conductivity and limited number of

active sites of NiO is a big barrier to capitalize it for practical applications. The  $\text{Co}_3\text{O}_4$ ,  $\text{NiCo}_2\text{O}_4$  and NiO do not match with the requirements in terms of catalytic site number, electrical conductivity, stability, and durability in order to use them for real time water electrolyzers.

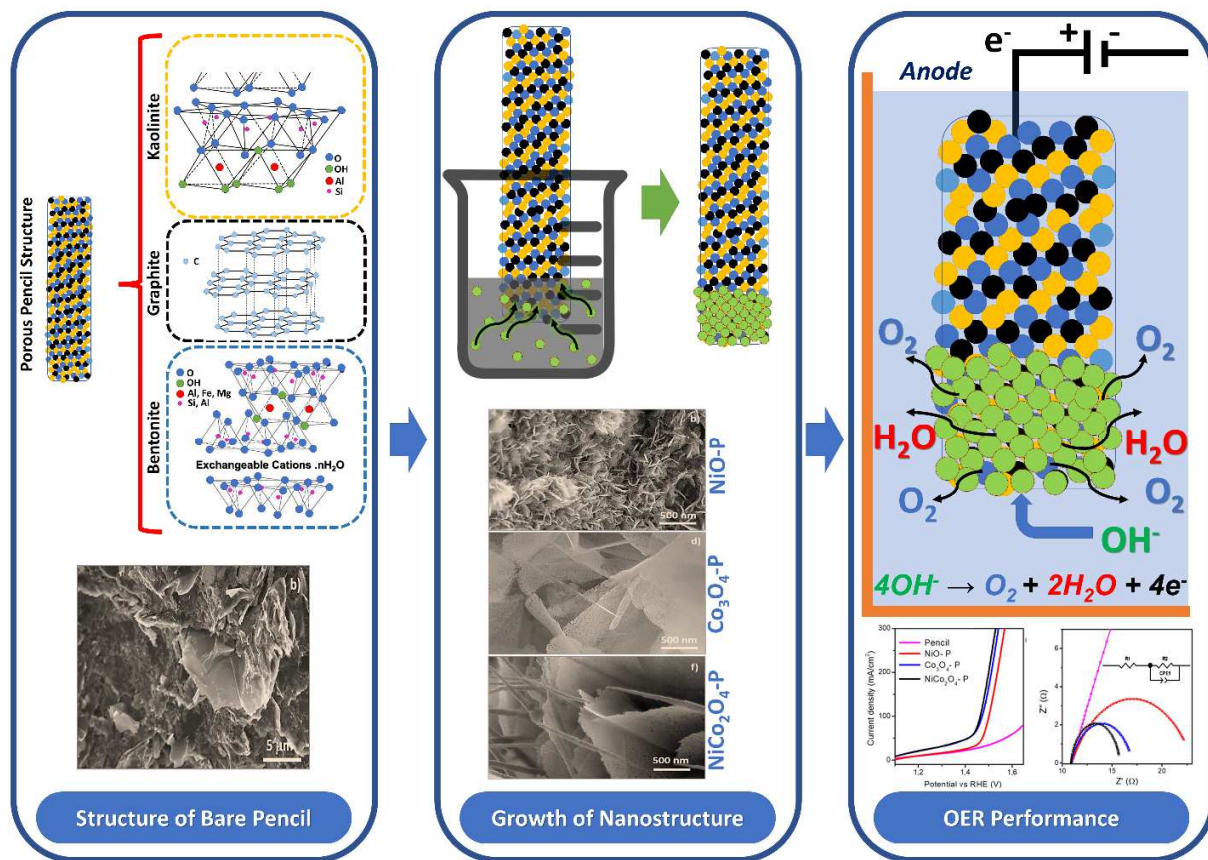
The material class of clay minerals such as bentonite and kaolinite have never been combined with metal oxides for superfast water catalysis. The bentonite and kaolinite have been found to be very active adsorbents because of their excellent specific surface area, pore size and anionic surface nature [51-54]. Moreover, the chemical composition of kaolinite (Kaol) ,  $\text{Al}_2\text{Si}_2\text{O}_5(\text{OH})_4$ , is associated with distinctive 1:1 layered structure formed by the stacking of Al-O octahedral and Si-O tetrahedral geometry [55]. The unique surface of kaolinite is consisting of several hydroxyl groups and they play a vital role in catalytic processes [56]. Kaolinite exhibits attractive surface features including hydrophilic surface, high surface area and considerable stability [57]. The density functional theory suggests that the presence of Al- hydroxyls in kaolinite surface shows a dynamic role in tuning the concentration of oxygen vacancies and  $\text{Co}^{2+}$  ions on  $\text{Co}_3\text{O}_4$  surface [15]. Therefore, considering these important aspects of bentonite and kaolinite for water catalysis, we have utilized them in the shape of PGR for the deposition of the most investigated  $\text{NiCo}_2\text{O}_4$ ,  $\text{Co}_3\text{O}_4$ , and NiO nanostructured materials for OER process. It is well established that the PGR are hybrid materials consisting approximately (65% graphite, 30% clay, 5% a binder (like wax, high polymer, or resins)) [58-63]. Such compounds with chemical composition, surface properties, catalytic properties, high porosity and high conductivity of PGR could be highly favorable for the OER. Also, the presence of Fe in the catalytic material can accelerate the OER activity [62].

The PGR is chemically and mechanically very stable and works at the wide range of potentials *i.e.*  $-0.8$  to  $0.8$ ,  $-1.0$  to  $0.8$ , and  $-0.8$  to  $0.6$  V versus saturate calomel electrode (SCE) in various electrolytic systems including  $\text{H}_2\text{SO}_4$ , KCl, and NaOH respectively compared to metallic electrodes such as (Au or Pt) [64]. The PGR is also a low cost electrode material among the carbon based electrodes which are utilized in the electroanalysis applications and its reported cost is 0.13 \$ which is several orders less than the cost of glassy carbon electrode (GCE) 190 \$ [65]. Therefore, the use of PGR as substrate and co-catalyst for the growth of metal oxide nanostructures and electrode is low cost and efficient electrode for the production of  $\text{O}_2$ . It is obvious that the bentonite and kaolinite have shown an excellent ability to host flower like morphology of NiO, thin nanosheets of  $\text{Co}_3\text{O}_4$  and mixture of nanowires/nanowalls of  $\text{NiCo}_2\text{O}_4$  in the current study. Both

the bentonite and kaolinite exhibit numerous catalytic centers, therefore they have been used as co-catalyst for the proposed metal oxide nanostructures.

We have found that native PGR shows the substantial OER activity relatively at high overpotential and high slope. However, the use of PGR as a substrate and co-catalyst has strongly enhanced the electrocatalytic properties of NiO, Co<sub>3</sub>O<sub>4</sub> and NiCo<sub>2</sub>O<sub>4</sub> electrocatalysts. Importantly, the microporosity of modified PGR has enabled the easily bubbling of O<sub>2</sub> during the measurements and enhanced the stability of electrode material for long term applications under harsh alkaline conditions.

In this work, we have developed alternative low-cost and high performance electrocatalysts. The combination of metal oxides with PGR offers particularly suitable chemical properties to surpassing OER. The proposed mechanism of the shown excellent electrochemical properties is based on the dynamic and unique chemical composition of clay minerals, and metal oxide nanostructures in the form of *in situ* composite electrode system. Moreover, an excellent electrical conductivity from graphite is favorable condition to improve the catalytic and electronic properties of Co<sub>3</sub>O<sub>4</sub>, NiCo<sub>2</sub>O<sub>4</sub> and NiO nanostructures towards water splitting. The specific surface area obtained from standard multi-point Brunner-Emmett-Teller theory (BET) method for bare graphite pencil, NiO/PGR, Co<sub>3</sub>O<sub>4</sub>/PGR, and NiCo<sub>2</sub>O<sub>4</sub>/PGR, was found to be 19.749 m<sup>2</sup> g<sup>-1</sup>, 21.711 m<sup>2</sup> g<sup>-1</sup>, 22.064 m<sup>2</sup> g<sup>-1</sup> and 23.359 m<sup>2</sup> g<sup>-1</sup> respectively. The pore volume for bare graphite pencil, NiO-P, Co<sub>3</sub>O<sub>4</sub>-P, and NiCo<sub>2</sub>O<sub>4</sub>-P exhibited a 0.084 cm<sup>3</sup> g<sup>-1</sup>, 1.110 cm<sup>3</sup> g<sup>-1</sup>, 1.239 cm<sup>3</sup> g<sup>-1</sup>, and 1.802 cm<sup>3</sup> g<sup>-1</sup> respectively was found. These experimental values about the surface area and pore volume confirm that the swift and easy transport of ions from the electrolyte through the pore size of graphite and clay minerals at the NiCo<sub>2</sub>O<sub>4</sub> electrode surface has favored the efficient oxidation/reduction reaction by producing the intense bubbling of O<sub>2</sub> gas through the porous structure of modified PGR electrode. Scheme 1 shows the graphical representation of structure of bare and metal oxide nanostructures modified PGR, and the OER activity of composite electrodes in 1.0 M KOH.



Scheme 1 Graphical view of the prepared metal oxide/PGR composite electrodes and their use for OER process

## 2. Results and discussion

In this study, we have grown  $\text{NiCo}_2\text{O}_4/\text{PGR}$ ,  $\text{Co}_3\text{O}_4/\text{PGR}$ , and  $\text{NiO}/\text{PGR}$  via a straightforward aqueous chemical growth method described in details in Supporting Information, section S1. The morphological and structural properties chemical composition and functionalities of the prepared catalysts, were systematically investigated by complementary techniques such as scanning electron microscopy (SEM), high-resolution transmission electron microscopy (HRTEM) and scanning transmission electron microscopy (STEM) combined with energy electron loss spectroscopy (EELS) and energy dispersive spectroscopy (EDS), X-ray diffraction (XRD), X-ray photoelectron spectroscopy (XPS), BET surface analyzer, and electrochemical measurements.

Figure 1 shows the OER overpotential of NiCo<sub>2</sub>O<sub>4</sub>/PGR compared to the reported outstanding OER catalysts [66--75]. The OER activity is found at the lowest overpotential of 234 mV at high current density of 100 mA cm<sup>-2</sup> in 1.0 M KOH aqueous solution for the NiCo<sub>2</sub>O<sub>4</sub>/PGR to date. Figure 1 is clearly showing the advancement in the field by introducing the new, facile, and low cost and earth abundant in situ architecture of electrocatalysts towards OER. The reported works have been found the most of the active OER catalysts, however they are produced by the complicated methods and rarely studied under the industrial electrolyzer conditions. In this view, the presented approach exhibits the lowest overpotentials and stability under the industrial electrolyzer conditions.

XRD analysis was carried out on the metal oxides deposited on the PGR (Figure 2). The bare pencil shows a typical graphitic peaks at 26.54° and 54.66° corresponding to (002) and (004) diffraction patterns, respectively. The crystal facets of MgO and SiO<sub>2</sub> expected from clay minerals were also identified in PGR. The reflections of MgO are completely supported by the reference card no: (96-901-3253) and the crystal facets of SiO<sub>2</sub> are well matched with the reference card no: (01-079-1910). The patterns of graphite are in good agreement with the reference card no: (03-065-6212). No other impurities or suspicious were determined by the XRD analysis. After the growth of onto the graphite pencil, the prominent reflections of Co<sub>3</sub>O<sub>4</sub>, NiCo<sub>2</sub>O<sub>4</sub>, and NiO were clearly identified (Figure 2). For the NiCo<sub>2</sub>O<sub>4</sub>/PGR, the crystal planes were identified as 111, 220, 331, 422, 511, 531, and 533. The crystal planes for the NiO/PGR were observed as 101, 012, 110, 113, and 006. The reflections of Co<sub>3</sub>O<sub>4</sub>/PGR were seen as 111, 022, 113, 222, 004, 224, 115, 244, 026 and 335. They are fully supported by the reference card no: [(96-900-5900), (01-073-1702), (00-044-1159)], respectively. The weak diffraction patterns of MgO, graphite carbon and SiO<sub>2</sub> are also recorded and they are in good agreement with the reference card no: [(96-901-3253), (01-079-1910), (03-065-6212)] as shown in Figure 2. Any other unidentified crystal facet was found in the metal oxide/PGR hybrid catalysts proving their high purity. The chemical composition of various prepared samples was quantified from XRD results using High Score Plus Software (Quantitative Rietveld analysis) to quantify the relative distribution of each component in each composite system shown in Supplementary Table 1. This analysis reveals that the amount of MgO, SiO<sub>2</sub> and graphite in each composite is almost constant, whereas the content of metal oxide nanostructures layer on the PGR is relatively low.

The *in situ* grown metal oxide nanostructures onto PGR were analyzed by SEM. The bare PGR is quite smooth with no particular nanostructures and only large platelets of clays can be observed as expected with some porous features (Supporting Information, Figure S1). While at low magnification (Supporting Information, Figure S2), no particular material structuration was observed except for PGR decorated with  $\text{Co}_3\text{O}_4$  and  $\text{NiCo}_2\text{O}_4$  for magnification of 10 kx (Figures S2d and S2f), high resolution (HR) SEM images reveal various nanostructures for the three designed catalysts (Figure 3). Successful synthesis of metal oxide nanostructures is of great importance for electrochemical processes thanks to the offered high surface and porosity. Interestingly, the growth at the PGR surface allowed to produce nanostructured metal oxides as observed with bulk synthesis approach [76,77]. NiO exhibit nanowalls forming flower-like structures (Figures 3a and 3b).  $\text{Co}_3\text{O}_4$  are composed of thin and large nanosheets (Figures 3c and 3d) and  $\text{NiCo}_2\text{O}_4$  are a mixed structure alternating large nanowalls and nanowires (Figures 3e and 3f). After the OER experiments, the observed nanostructures are basically preserved except for  $\text{NiCo}_2\text{O}_4/\text{PGR}$  for which the very thin nanowalls seem less stable and they probably dissolve during the electrochemical experiments (Supplementary Information, Figure S3).

The carried out EDS analysis of PGR has confirmed the successful chemical composition of raw PGR, NiO/PGR,  $\text{Co}_3\text{O}_4/\text{PGR}$  and  $\text{NiCo}_2\text{O}_4/\text{PGR}$  (Supplementary Information, Figures S4 and Supplementary Table 2). It is worth to notice that chemical composition of the nanostructured composites was found comparable even after the long term electrolysis.

XPS is an essential and powerful tool to investigate the chemical composition and the oxidation states of metal oxides. The three designed electrocatalysts were analyzed by XPS (Figure 4). The Ni 2p spectral region of NiO-PGR confirms the signature of NiO with the typical doublet structure (Figure S5a) and the Ni  $2p_{3/2}$  feature showing a main line and its satellite at  $\sim 861$  eV (Figure 4a). The main feature of Ni  $2p_{3/2}$  shows the  $\text{Ni}^{2+}$  and the  $\text{Ni}^{3+}$  contribution typically centered at 853.5 eV (NiO) and 855.3 eV ( $\text{Ni}_2\text{O}_3$ ), respectively, in good agreement with the literature [78-80]. From deconvolution, the  $\text{Ni}^{2+} / \text{Ni}^{3+}$  ratio was estimated to be 0.36. As expected, the O 1s profile of NiO/PGR exhibits two peaks at 529.3 and 531.0 eV (Figure 4b). They are respectively assigned to the metal-oxygen bonds and singly charged oxygen vacancies [81, 15]. The amount of oxygen vacancies in the NiO/PGR was found to be of 33 %.

For  $\text{Co}_3\text{O}_4/\text{PGR}$ , Co 2p and O 1s spectra are shown in Figures 4c and 4d (the 2p spectral region  $\text{Co}_3\text{O}_4/\text{PGR}$  is shown in Figure S4b). Co  $2p_{3/2}$  doublet was well fitted by the tetrahedral  $\text{Co}^{3+}$  (779.4

eV) and octahedral  $\text{Co}^{2+}$  (780.4 eV) contributions [80-82].  $\text{Co}^{3+}/\text{Co}^{2+}$  ratio is found to be  $\sim 0.27$ . The O 1s peak was de-convoluted into two peaks positioned at 529.8 and 530.9 eV which corresponds to the Co-O bonds and oxygen vacancies, respectively [83]. The  $\text{Co}_3\text{O}_4/\text{PGR}$  electrode exhibits 49 % of oxygen vacancies.

De-convolution of Co  $2p_{3/2}$ , Ni  $2p_{3/2}$  and O 1s signals of  $\text{NiCo}_2\text{O}_4/\text{PGR}$  shows the main spectral signatures expected for this  $\text{NiCo}_2\text{O}_4$  (Figures 4e, 4f and 4g, the full spectral domain of Co 2p and Ni 2p is shown in Figures S5c and S5d) [84-86]. The Ni  $2p_{3/2}$  feature was fitted by four components corresponding to the  $\text{Ni}^{2+}$  ions at 853.8 eV, the  $\text{Ni}^{3+}$  ions at 855.4 eV and the shake-up satellite peak deconvoluted with two lines (861.0 and 866.2 eV). The main lines from the Co  $2p_{3/2}$  fits are as well consistent with  $\text{Co}^{3+}$  (779.2 eV) and  $\text{Co}^{2+}$  (280.2 eV) species usually found for  $\text{NiCo}_2\text{O}_4$  oxide. From the respective area feature,  $\text{Ni}^{2+}/\text{Ni}^{3+}$  and  $\text{Co}^{3+}/\text{Co}^{2+}$  ratios have been found around 0.19 and 0.37, respectively. The high  $\text{Ni}^{2+}/\text{Ni}^{3+}$  and  $\text{Co}^{3+}/\text{Co}^{2+}$  ratios in the  $\text{NiCo}_2\text{O}_4/\text{PGR}$  has revealed dynamic contribution towards enhanced OER activity. The O 1s spectra recorded from  $\text{NiCo}_2\text{O}_4/\text{PGR}$  materials could be well fitted with two oxygen contributions corresponding to binding energies of 529.4 and 530.9 eV corresponding to the O-Ni/Co bonds and the oxygen vacancies, respectively. The quantified 52 % of oxygen vacancies was observed in the  $\text{NiCo}_2\text{O}_4/\text{PGR}$  sample.

We report here detailed characterizations at the atomic scale of  $\text{NiCo}_2\text{O}_4/\text{PGR}$  before and after OER experiments by HRTEM and scanning transmission electron microscopy (STEM) combined with EELS and EDS. HRTEM micrographs reveal that  $\text{NiCo}_2\text{O}_4$  clusters are highly crystallized either before or after OER experiments (Figures 5a-5b,5g-5h). The spacing distances  $d_{hkl}$  obtained from the Fast Fourier Transform (FFT) patterns (insert Figures 3b and 3h) correspond to the cubic structure of  $\text{NiCo}_2\text{O}_4$  in agreement with XRD experiments (Fdm,  $a = b = c = 8.1 \text{ \AA}$ ). Additionally, EELS maps show that Ni, Co and O are homogeneously distributed within the particles for both samples (Figures 5d-5f and 5j-5l). The TEM images at different magnifications are enclosed in the Supplementary Information, Figure S6. They provide the local morphological features of  $\text{NiCo}_2\text{O}_4/\text{PGR}$  before the OER analysis. These images show that the  $\text{NiCo}_2\text{O}_4/\text{PGR}$  is mainly composed of nanoparticles with size of 10 nm which certainly facilitate the easy access of catalyst surface for the water splitting reaction. Furthermore, the shape of nanowalls and needles at higher scale is highly favorable for the transport of charges during the water catalysis. Supplementary EDS experiments were done over larger areas of the samples and they are in complete agreement

with EELS results (Figures S7a-S7f). These in-depth structural and elemental analysis demonstrates the high stability of the designed electrocatalyst.

The nanostructured electrocatalyst performance is extremely dependent on the porosity and particle/pore size of the electrocatalyst. The specific surface area and the pore-size distribution of the bare graphite pencil, NiO/PGR, Co<sub>3</sub>O<sub>4</sub>/PGR, and NiCo<sub>2</sub>O<sub>4</sub>/PGR nanostructures were calculated by nitrogen gas adsorption experiments; as shown in Figure 6. A type-II isotherm was obtained for all nanostructures, the presence of macropores the isotherm rises rapidly near P/P<sub>0</sub> = 1 and in the limit of large macropores may exhibit an essentially vertical rise. Therefore, it is anticipated that the NiO/PGR, Co<sub>3</sub>O<sub>4</sub>/PGR, and NiCo<sub>2</sub>O<sub>4</sub>/PGR have larger macroporous structures. Furthermore, NiO/PGR, Co<sub>3</sub>O<sub>4</sub>/PGR, and NiCo<sub>2</sub>O<sub>4</sub>/PGR isotherms reveal Type H3 hysteresis which is due to the non-rigid aggregates of plate-like particles and slit-shaped pores. These results are in agreement with the SEM results. The specific surface area, calculated using the standard multi-point BET method for bare graphite pencil, NiO/PGR, Co<sub>3</sub>O<sub>4</sub>/PGR, and NiCo<sub>2</sub>O<sub>4</sub>/PGR, was found to be 19.749 m<sup>2</sup> g<sup>-1</sup>, 21.711 m<sup>2</sup> g<sup>-1</sup>, 22.064 m<sup>2</sup> g<sup>-1</sup> and 23.359 m<sup>2</sup> g<sup>-1</sup> respectively. Bare graphite pencil, NiO-P, Co<sub>3</sub>O<sub>4</sub>/PGR, and NiCo<sub>2</sub>O<sub>4</sub>/PGR exhibited a 0.084 cm<sup>3</sup> g<sup>-1</sup>, 1.110 cm<sup>3</sup> g<sup>-1</sup>, 1.239 cm<sup>3</sup> g<sup>-1</sup>, and 1.802 cm<sup>3</sup> g<sup>-1</sup>, pore volume, respectively (inset of Figure 6). This suggested that the NiCo<sub>2</sub>O<sub>4</sub>/PGR composite accelerated the OER activity due to its high specific surface area [87-90].

## 2.1. Half-cell OER characterization

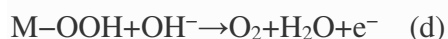
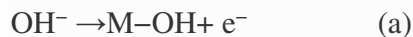
The exposure of hydroxyl groups from highly porous clay structure enabled favorable interaction with metallic ions during the growth process and consequently a compatible metal oxide-PGR composite is prepared. The prepared composite electrodes have several unique features for electro catalytic applications such as high specific surface area, multiple number of active sites, excellent electrical conductivity, high metal oxide-PGR compatibility, abundant oxygen vacancies, higher oxidation states of transition metallic ions and large porosity. The electrocatalytic activities of bare graphite pencil and NiCo<sub>2</sub>O<sub>4</sub>/PGR, Co<sub>3</sub>O<sub>4</sub>/PGR, and NiO/PGR were evaluated in 1.0 M KOH aqueous solution as shown in Figure 7. The *in situ* grown Co<sub>3</sub>O<sub>4</sub> and NiCo<sub>2</sub>O<sub>4</sub> on graphite pencil have shown an excellent OER activity with a large current density and the lowest overpotential than the other catalysts as shown in Figure 1. The NiCo<sub>2</sub>O<sub>4</sub>/PGR, Co<sub>3</sub>O<sub>4</sub>/PGR, and NiO/PGR produce a current density of 100 mA cm<sup>-2</sup> at an overpotential of 234 mV, 242 mV, and 272 mV,

respectively. The PGR exhibits a high porosity which enables the ionic charges flow at the applied potential which might create a current prior to the OER onset potential as shown in Figure 7. The bare PGR needs an overpotential of 441 mV to produce a current density of  $100 \text{ mA cm}^{-2}$ . The overpotential analysis suggests that the  $\text{NiCo}_2\text{O}_4/\text{PGR}$ , and  $\text{Co}_3\text{O}_4/\text{PGR}$  have 38 mV, 30 mV lower overpotential at a current density of  $100 \text{ mA cm}^{-2}$  in 1.0 M KOH than NiO/PGR catalyst. The high  $\text{Ni}^{2+}/\text{Ni}^{3+}$  and  $\text{Co}^{3+}/\text{Co}^{2+}$  ratios and 52 % of oxygen vacancies in the composition of  $\text{NiCo}_2\text{O}_4/\text{PGR}$  have favored improved OER performance. It has been proved that the high content of  $\text{Co}^{3+}$  in the cobalt based catalysts can enhance the OER because  $\text{Co}^{3+}$  ions provide a high probability for the adsorption of electrophilic species and consequently they facilitate of oxygen in the  $\text{OH}^-$  ions<sup>73,74</sup>. Furthermore, the main challenge of blockage of oxygen gas inside the catalyst surface is resolved by the proposed PGR based material due to its large pore volume which easily bubble out the oxygen gas without the deactivation of catalytic material as clearly described by BET results. Therefore, the modified PGR electrode can be used for the long term applications. The  $\text{NiCo}_2\text{O}_4/\text{PGR}$  electrode is associated with large specific surface area and pore volume of  $23.359 \text{ m}^2 \text{ g}^{-1}$  and  $1.802 \text{ cm}^3 \text{ g}^{-1}$  respectively and they have played a vital in accelerating the OER kinetics and stability. The high specific surface of area of  $\text{NiCo}_2\text{O}_4/\text{PGR}$  has provided the large exposure of active centers for the catalytic reaction, therefore an excellent OER activity is demonstrated [91, 61]. Furthermore, the modification of PGR with nanostructured materials is associated with the high specific surface area, electrocatalytic properties and good conductivity compared to the bare PGR, thus an enhanced electrochemical activity is observed [92]. The XRD study has revealed the presence of  $\text{SiO}_2$  and  $\text{MgO}$  in the bare and modified PGR electrodes which have been shown to significantly impact the electrocatalytic performance. The reactive distribution of  $\text{SiO}_2$ ,  $\text{MgO}$  and graphite from the XRD results in each composite system was found nearly same, indicating that most of the catalytic activity towards OER was coming from layer of nanostructured metal oxides. But, at the same time we have seen in the literature that the  $\text{SiO}_2$  and  $\text{MgO}$  have played role in lifting the catalytic activity, therefore in our composite systems their role was identified as co-catalyst for various metal oxide nanostructures. The silica material has tendency to allow the water molecules due to its high wettability which further gives out an active oxide layer with high porosity structure [93]. This high porosity of active oxide coating features within the bulk depth of PGR electrode and lead to the enhanced electrocatalytic performance. The high surface energy of silica from the PGR and interlocked structure between the NiO,  $\text{Co}_3\text{O}_4$ ,  $\text{NiCo}_2\text{O}_4$

and inactive silica reveal the excellent adhesion [94]. The presence of silica in the electrode not only improve the catalytic properties but it also increases the durability towards long term applications [94]. Beside this, a certain amount of MgO in the electrode is essential to produce a high amount of oxygen vacancies via induced defects engineering [95] and abundant concentration of  $\text{Co}^{3+}$  ions. The presence of MgO within the composition of composite systems could provide defects and edges, thereby it enhanced the OER activity of metal oxide nanostructures [95]. The oxygen vacancies have been shown to decrease the adsorption energy of water molecules and become responsible for the weakening of metal-oxygen bonds to provide the favorable environment for the exchange of short lived species and electrons, therefore enhancing the OER reaction [96, 97]. Furthermore, the presence of iron from bentonite in the composite systems favored the superior OER activity [62].

This outstanding performance of  $\text{NiCo}_2\text{O}_4/\text{PGR}$ ,  $\text{Co}_3\text{O}_4/\text{PGR}$ , and  $\text{NiO}/\text{PGR}$  is attributed to the unique features of fabricated electrode consisting clay minerals, graphite, and metal oxide nanostructures. For the better pictorial presentation of obtained overpotential values at  $100 \text{ mA cm}^{-2}$  and they are plotted against the electrode materials such as bare pencil,  $\text{NiCo}_2\text{O}_4$ ,  $\text{Co}_3\text{O}_4$ , and  $\text{NiO}$  composite materials as shown in Figure 7b. Further to add, the nanowires like morphology in case of  $\text{NiCo}_2\text{O}_4$  onto pencil graphite is guiding the electrochemical reaction at favorable kinetics, thus low overpotential was observed. The OER kinetics on the surface of  $\text{NiCo}_2\text{O}_4/\text{PGR}$ ,  $\text{Co}_3\text{O}_4/\text{PGR}$ , and  $\text{NiO}/\text{PGR}$  systems was evaluated by Tafel plots under alkaline conditions. The  $\text{NiCo}_2\text{O}_4$  composite material exhibits a Tafel slope of  $110 \text{ mVdec}^{-1}$ ,  $\text{Co}_3\text{O}_4$  composite possesses a Tafel slope of  $132 \text{ mVdec}^{-1}$  and  $\text{NiO}$  composite has shown Tafel slope of  $115 \text{ mVdec}^{-1}$  as shown in Figure 7c. The obtained Tafel slopes are slightly higher due to several reasons such as microstructure of electrode and the composition of electrode. The OER mechanism is not well understood in the literature, however generally it involves the 4-electron transfer process and followed by the high energy barrier of overpotential [98,99]. In the alkaline electrolytic conditions, the OER takes place through the oxidation of adsorbed hydroxyl anion on the metal active center with the formation of  $\text{M-OH}$  specie as shown in equation (a). Afterwards, the proton and electron are taken away from the  $\text{M-OH}$  to give out  $\text{M-O}$  as shown in equation (b). The formation of molecular oxygen is followed by either of the two pathways. In one pathway,  $\text{M-O}$  interacts with a hydroxyl anion to produce hydroperoxide  $\text{M-OOH}$ , then proton- electron couple transfer step takes place with the release of molecular oxygen as shown in equation (c) and (d) [100, 101]. In

the second pathway, the direct association of two M-O intermediates gives out the molecular oxygen as shown in equation (e) [102].



The Tafel slopes for these composite materials are estimated from the region of large current densities, therefore the measured value of Tafel slope is slightly higher. Another reason for the high value of Tafel slope is inherently assigned to the insulation offered by the clay minerals in the modified electrode. This analysis again opens, new domains for the future studies on the optimization of clay composition in the PGR in order to bring Tafel value at low magnitude which will further facilitate the understanding of OER mechanism in alkaline electrolytic conditions. To understand the reason for the significant OER activity of newly prepared composite materials NiCo<sub>2</sub>O<sub>4</sub>/PGR, Co<sub>3</sub>O<sub>4</sub>/PGR, and NiO/PGR, the electrochemically active surface area (ECSA) was calculated as it can be a good indicator for the evaluation of significant changes at the interface of electrode [80,81]. The ECSA was calculated from the non-Faradic region of CV curves at various scan rates in 1.0 M KOH (Supplementary Information, Figure S8). The material with higher value of ECSA exhibits a superior electrocatalytic activity because of the large surface area and high exposure of catalytic sites during electrocatalysis. The NiCo<sub>2</sub>O<sub>4</sub>/PGR, Co<sub>3</sub>O<sub>4</sub>/PGR, and NiO/PGR possess an ECSA of 736.1 μFcm<sup>-2</sup>, 522.2 μFcm<sup>-2</sup>, and 223 μFcm<sup>-2</sup> respectively as shown in Figure 7d. The bare graphite pencil exhibits an ECSA value of 142.9 μFcm<sup>-2</sup>. It is obvious from ECSA values that the composite materials have an excellent electrocatalytic activities due to higher surface area compared to the pristine metal oxides. Figure 7e shows a multistep

chronopotentiometric response of NiCo<sub>2</sub>O<sub>4</sub>/PGR, Co<sub>3</sub>O<sub>4</sub>/PGR, and NiO/PGR with a starting current density of 100 mA cm<sup>-2</sup> to 450 mA cm<sup>-2</sup> (100 and 50 mA cm<sup>-2</sup> per 500 s) in 1.0 M KOH. The potentials became immediately leveled off at 1.46 V, 1.47 V and 1.50 V for NiCo<sub>2</sub>O<sub>4</sub>/PGR, Co<sub>3</sub>O<sub>4</sub>/PGR, and NiO/PGR respectively at the beginning of current value and remained unchanged for 500 s and other steps also demonstrated the same behavior indicating an excellent electrical conductivity, mechanical activity and mass transfer of NiCo<sub>2</sub>O<sub>4</sub>/PGR, Co<sub>3</sub>O<sub>4</sub>/PGR, and NiO/PGR. It is worth to see that the rough line at higher current densities that of 100 mA cm<sup>-2</sup> is suggesting the swift bubbling of gas during the OER processes. But it is not much intense which indicates that the produced oxygen is successfully removed from the surface due to the porous nature of electrode where oxygen bubble produced inside the porous catalyst structure is evacuated with negligible limitation factor offered by porous throat. The multistep potential curves were recorded for the NiCo<sub>2</sub>O<sub>4</sub>/PGR, Co<sub>3</sub>O<sub>4</sub>/PGR, and NiO/PGR in 1.0M KOH as shown in Figure 7f and they have fully supported the results shown in Figure 7e. The enhanced electrocatalytic activity of NiCo<sub>2</sub>O<sub>4</sub>/PGR, Co<sub>3</sub>O<sub>4</sub>/PGR, and NiO/PGR was further elucidated by electrochemical impedance spectroscopy (EIS) in 1.0M KOH aqueous solution. Figure 7g represents the Nyquist plots of NiCo<sub>2</sub>O<sub>4</sub>/PGR, Co<sub>3</sub>O<sub>4</sub>/PGR, and NiO/PGR, thereby the charge transfer resistance (R<sub>ct</sub>) of prepared materials between the interface of electrode and electrolyte was quantified. The R<sub>ct</sub> of NiCo<sub>2</sub>O<sub>4</sub>/PGR, Co<sub>3</sub>O<sub>4</sub>/PGR, and NiO/PGR in OER was found in the order of 4.87, 6.15, and 12.25 Ω cm<sup>2</sup> respectively. However, a large charge transfer resistance of bare pencil 306.9 Ω cm<sup>2</sup> in OER was observed. The charge transfer of bare pencil graphite rod is higher than three composite samples due to fact that the nanostructured materials have better electron communication due to quantum confinement effect. Further to add, the nanowires like morphology in case of NiCo<sub>2</sub>O<sub>4</sub> onto pencil graphite is guiding the electrochemical reaction at favorable kinetics. The quantum confinement effect is well established in the literature when the electrical communication features are described. These results verify the feasibility of swift electron transport in the composite samples compare to the bare graphite pencil due to the mutual contribution of electrical conductivity from semiconducting metal oxides and graphite. In concise, the enhanced catalytic activity of composite materials in OER can be associated to the different combined effects of increased electrical, surface and chemical properties in the composite materials that successfully capitalize the OER features at the same time. Before and after the durability test, the LSV curves were found stable for the composite materials NiO, Co<sub>3</sub>O<sub>4</sub>, and

NiCo<sub>2</sub>O<sub>4</sub> without any loss of current density and onset potential as shown in Figure 8a,b,c. The long term durability of composite materials NiO, Co<sub>3</sub>O<sub>4</sub>, and NiCo<sub>2</sub>O<sub>4</sub>, was also studied at constant current density of 100 mA cm<sup>-2</sup> in 1.0 M KOH and no any abrupt change in the overpotential was recorded for the time period of 60 h as shown in Figure 8d,e,f. These stability results suggest that the NiCo<sub>2</sub>O<sub>4</sub>/PGR, Co<sub>3</sub>O<sub>4</sub>/PGR, and NiO/PGR electrodes are capable to work for long term applications and the structural and compositional studies were also carried out after the durability measurements. All the modified electrodes have maintained the morphology and composition after durability test as shown in Figure S3 and S4 respectively. The NiCo<sub>2</sub>O<sub>4</sub>/PGR electrocatalyst before and after the OER experiment was further studied in term of morphology and composition by the HRTEM and EELS. The obtained results revealed the high durability and stability of material without the loss of morphology and composition during long term OER testing as shown in Figure S7. The stability and durability of composite electrodes could be attributed to high metal oxide-PGR compatibility and easy bubbling of O<sub>2</sub> gas through the porous structure which did not change or damage the composition and morphology of composite electrodes.

The concentration of electrolyte has significant effect on the current density, overpotential and stability of electrocatalyst towards any electrolysis process. It has been known that highly alkaline electrolyte strongly decrease the activity and stability of nonprecious metal oxides based electrocatalysts for OER reaction. For this reason, we have investigated the role of KOH electrolytic concentration on the performance of presented metal oxides decorated on the PGR. The two concentrations of electrolyte were selected such as 0.1 M KOH and 6.0 M KOH. The purpose of using 0.1 M KOH was to see effect on the catalytic activity of the NiCo<sub>2</sub>O<sub>4</sub>/PGR, Co<sub>3</sub>O<sub>4</sub>/PGR, and NiO/PGR electrodes, however the use of 6.0 M KOH electrolytic concentration was to monitor the performance of each catalyst under industrial electrolyzer conditions. This study could help us to identify the most efficient material for the industrial oxygen production. The LSV curves were measured for NiCo<sub>2</sub>O<sub>4</sub>/PGR, Co<sub>3</sub>O<sub>4</sub>/PGR, and NiO/PGR at a scan rate of 5 mV/s in 0.1 M KOH see Supplementary Information, Figure S9). The calculated overpotentials at 30 mA cm<sup>-2</sup> for the NiCo<sub>2</sub>O<sub>4</sub>/PGR, Co<sub>3</sub>O<sub>4</sub>/PGR, and NiO/PGR were 290 mV, 310 mV and 330 mV respectively. This suggests that the electrolyte concentration has significant influence on the current density, overpotential and stability of electrocatalyst, therefore it will provide a guideline that the proposed materials could be tested at the higher alkaline electrolyte concentrations.

Therefore, we have also investigated the catalytic activities of NiCo<sub>2</sub>O<sub>4</sub>/PGR, Co<sub>3</sub>O<sub>4</sub>/PGR, and NiO/PGR under 6.0 M KOH electrolytic conditions as shown in Figure 8a. These newly prepared NiCo<sub>2</sub>O<sub>4</sub>/PGR, Co<sub>3</sub>O<sub>4</sub>/PGR, and NiO/PGR have shown the lowest overpotentials of 210 mV, 220 mV, and 250 mV respectively for a current density of 150 mA cm<sup>-2</sup> as shown in Figure 9a. The concentration of an electrolyte has significantly decreased the overpotential and increased the current density of NiCo<sub>2</sub>O<sub>4</sub>/PGR, Co<sub>3</sub>O<sub>4</sub>/PGR, and NiO/PGR composite materials in 6.0 M KOH solution. This indicates an outstanding OER activities of newly proposed electrodes and provide an easy access of these efficient materials for industrial applications. The NiCo<sub>2</sub>O<sub>4</sub>/PGR exhibits a superior performance than the other composite electrode materials due to favorable electronic environment of bi-metal ions and larger surface area. The NiCo<sub>2</sub>O<sub>4</sub>/PGR has lower effective current density value due to its large size, thus we see a low overpotential for it.

The temperature has significant effect on the activity of electrocatalysts. Moreover, the effect of temperature on the electrocatalytic activity of these composite catalysts was also studied. It was also found that the OER activity of these composite materials in 6.0M KOH was highly enhanced at a high temperature of 60 °C and the NiCo<sub>2</sub>O<sub>4</sub>/PGR, Co<sub>3</sub>O<sub>4</sub>/PGR, and NiO/PGR required a lower overpotential of 160 mV, 180 mV, and 210 mV, respectively to achieve a current density of 250 mA cm<sup>-2</sup> as shown in Figures 9b-9d. The steady-state performance and durability of NiCo<sub>2</sub>O<sub>4</sub>/PGR, Co<sub>3</sub>O<sub>4</sub>/PGR, and NiO/PGR was also evaluated by multiple current steps chronopotentiometry experiments in 6.0 M KOH. It can be seen from Figure 9e, the variation in the increment of applied potential was recorded when the electrocatalytic current density was lifted to higher value ranging from 150 to 900 mA cm<sup>-2</sup>. At the initial step, the 150 mA cm<sup>-2</sup> was leveled off by the overpotential of 1.44 V, 1.45 V, and 1.48 V for the NiCo<sub>2</sub>O<sub>4</sub>/PGR, Co<sub>3</sub>O<sub>4</sub>/PGR, and NiO/PGR respectively and remains static for the time interval of 500 s. The increasing multiple current steps guided to keep overpotentials constant at a higher value than that of 150 mA cm<sup>-2</sup>. Also, the multistep potential experiment was conducted in order to verify the results shown in Figure 9f and the obtained results successfully demonstrated close in agreement for achieving the desired overpotential at specific current density. These catalytic activities reveal the outstanding performance, mass transport features and intrinsic excellency of NiCo<sub>2</sub>O<sub>4</sub>/PGR, Co<sub>3</sub>O<sub>4</sub>/PGR, and NiO/PGR during the long term OER electrolysis.

### 3. Conclusions

We have used pencil graphite rod with favorable properties for OER which are summarized as: 1. Iron active centers from bentonite played a drastic role in enhancing OER activity of NiCo<sub>2</sub>O<sub>4</sub>, Co<sub>3</sub>O<sub>4</sub>, and NiO, 2. The bentonite and kaolinite are associated with attractive surface properties, thermal and structural stability, which effectively hosted the NiCo<sub>2</sub>O<sub>4</sub>, Co<sub>3</sub>O<sub>4</sub>, and NiO nanostructures, 3. The graphite has driven the electrical conductivity of PGR modified with NiCo<sub>2</sub>O<sub>4</sub>, Co<sub>3</sub>O<sub>4</sub>, and NiO. The measured low overpotential of 234 mV at high current density of 100 mA cm<sup>-2</sup> for NiCo<sub>2</sub>O<sub>4</sub>/PGR in 1.0 M KOH aqueous solution demonstrates a significant OER activity for a nonprecious material. The large pore volume of NiCo<sub>2</sub>O<sub>4</sub>/PGR prevents the blockage of oxygen gas due to the porosity of modified electrode which easily bubbled out produced oxygen gas without the loss of activity of composite catalyst and its stability during OER process, therefore it can be used for long term applications. The superior performance of these composites towards OER is due to high surface to volume ratio due to nanostructured metal oxides and microporosity of PGR, high density of active sites contributed from clay minerals of PGR and metal oxides. The multi-step durability using both chronoamperometry and chronopotentiometry revealed the unseen role of bentonite and kaolinite in the enhancement of OER activities. Moreover, the optimization of bentonite, kaolinite and graphite ratio in the composition of PGR can even lower the overpotential of OER compared to the obtained values. The naturally inherent presence of SiO<sub>2</sub> favors the catalytic properties and durability of the electrode whereas the MgO produces the abundant oxygen vacancies and Co<sup>3+</sup> ions. The presence of large number of oxygen vacancies through SiO<sub>2</sub> and MgO, high Ni<sup>2+</sup>/Ni<sup>3+</sup> and Co<sup>3+</sup>/Co<sup>2+</sup> ratios, multi metal centers, large specific surface area, high pore volume, high electrochemical active surface area and fast charge transport within the NiCo<sub>2</sub>O<sub>4</sub>/PGR became the main reasons for its superfast OER kinetics. The proposed strategy of fabrication of low cost, earth abundant, efficient and stable catalysts for OER and other electrochemical applications can be considered as a promising and alternative guideline.

### **Acknowledgments**

We would like to thank the platform “Spectroscopies et Microscopies des Interfaces” (Laboratory of Physical Chemistry and Microbiology for Materials and the Environment, LCPME, Nancy, France) and A. Renard, Dr. M. Mallet (LCPME) for XPS analysis. B.V. thanks the platform “Microscopies, Microprobes and Metallography (3M)” (Institut Jean Lamour, IJL, Nancy, France)

and Dr. J. Ghanbaja for fruitful discussions. We also wish to thank Researchers Supporting Project number (RSP-2021/55) at King Saud University, Riyadh, Saudi Arabia.

#### **Declaration Statement**

Authors declare that the presented work is original and only considered for this journal.

#### **Data Availability Statement**

The processed data required to reproduce these findings cannot be shared at this time due to technical or time limitations.

#### **4. References**

- [1] Park J, Kwon T, Kim J, Jin H, Kim H Y, Kim B, et al. Hollow nanoparticles as emerging electrocatalysts for renewable energy conversion reactions, *Chem. Soc. Rev.* 2018; 47: 8173-8202.
- [2] Roy C, Sebok B, Scott B, Fiordaliso EM, Sørensen JE, Bodin A, et al. Impact of nanoparticle size and lattice oxygen on water oxidation on  $\text{NiFeO}_x\text{H}_y$ . *Nature Catalysis.* 2018; 1: 820-829.
- [3] Guan J, Duan Z, Zhang F, Kelly S D, Si R, Dupuis M, et al. Water oxidation on a mononuclear manganese heterogeneous catalyst. *Nature Catalysis.* 2018; 1: 870-877.
- [4] Wang H, Cui Y. Nanodiamonds for energy. *Carbon Energy.* 2019;1:13-8.
- [5] Ali A, Shen PK. Nonprecious metal's graphene-supported electrocatalysts for hydrogen evolution reaction: Fundamentals to applications. *Carbon Energy.* 2019;2:99-121.
- [6] Wu Z, Zhao Y, Jin W, Jia B, Wang J, Ma T. Recent Progress of Vacancy Engineering for Electrochemical Energy Conversion Related Applications. *Adv Funct Mater.* 2020;31:2009070.
- [7] Wang Y, Sun Y, Yan F, Zhu C, Gao P, Zhang X, et al. Self-supported NiMo-based nanowire arrays as bifunctional electrocatalysts for full water splitting. *Nano Energy.* 2018; 44: 353-363.
- [8] Yang Y, Lin Z, Gao S, Su J, Lun Z, Xia G, et al. Tuning Electronic Structures of Nonprecious Ternary Alloys Encapsulated in Graphene Layers for Optimizing Overall Water Splitting Activity. *ACS Catal.* 2017; 7: 469-479.
- [9] Papaderakis A, Tsiplakides D, Balomenou S, Sotiropoulos S. Electrochemical impedance studies of IrO<sub>2</sub> catalysts for oxygen evolution. *Journal of Electroanalytical Chemistry.* 2015; 757 ( ), 216-224.
- [10] Audichon T, Mayousse E, Morisset S, Morais C, Comminges C, Napporn TW, et al. Electroactivity of RuO<sub>2</sub>-IrO<sub>2</sub> mixed nanocatalysts toward the oxygen evolution reaction in a

water electrolyzer supplied by a solar profile. *International Journal of Hydrogen Energy*. 2014; 39: 16785-16796.

[11] Huang Z-F, Song J, Du Y, Xi S, Dou S, Nsanzimana JMV, et al. Chemical and structural origin of lattice oxygen oxidation in Co-Zn oxyhydroxide oxygen evolution electrocatalysts. *Nature Energy*. 2019; 4: 329-338.

[12] Wu T, Sun S, Song J, Xi S, Du Y, Chen B, et al. Iron-facilitated dynamic active-site generation on spinel  $\text{CoAl}_2\text{O}_4$  with self-termination of surface reconstruction for water oxidation. *Nature Catalysis*. 2019; 2: 763-772.

[13] Zhou Y, Sun S, Song J, Xi S, Chen B, Du Y, et al. Enlarged  $\text{Co-O}$  Covalency in Octahedral Sites Leading to Highly Efficient Spinel Oxides for Oxygen Evolution Reaction. *Advanced Materials*. 2018; 30: 1802912.

[14] Bergmann A, Martinez-Moreno E, Teschner D, Chernev P, Gliech M, de Araújo JF, et al. Reversible amorphization and the catalytically active state of crystalline  $\text{Co}_3\text{O}_4$  during oxygen evolution. *Nature Communications*. 2015; 6: 8625.

[15] Zhao Q, Fu L, Jiang D, Ouyang J, Hu Y, Yang H, et al. Nanoclay-modulated oxygen vacancies of metal oxide. *Commun Chem*. 2019; 2: 1-10.

[16] Kumar J P, Giri SD, Sarkar A. Mesoporous  $\text{NiO}$  with different morphology: Synthesis, characterization and their evaluation for oxygen evolution reaction. *International Journal of Hydrogen Energy*, 2018; 43: 15639-15649.

[17] Peng H, Ren J, Wang Y, Xiong Y, Wang Q, Li Q, et al. One-stone, two birds: Alloying effect and surface defects induced by Pt on  $\text{Cu}_{2-x}\text{Se}$  nanowires to boost C-C bond cleavage for electrocatalytic ethanol oxidation. *Nano Energy*. 2021;88:106307.

[18] Govatsi K, Seferlis A, Yannopoulos SN, Neophytides SG. The photo-electrokinetics of the  $\text{O}_2$  evolution reaction on  $\text{ZnO}$  nanorods. *Electrochimica Acta*. 2019; 298: 587-598.

[19] Zhang Y, Ouyang B, Xu J, Jia G, Chen S, Rawat RS, et al. Rapid Synthesis of Cobalt Nitride Nanowires: Highly Efficient and Low-Cost Catalysts for Oxygen Evolution. *Angewandte Chemie*. 2016;55:8670-4.

[20] Tong X, Xia X, Guo C, Zhang Y, Tu J, Fan HJ, et al. Efficient oxygen reduction reaction using mesoporous Ni-doped  $\text{Co}_3\text{O}_4$  nanowire array electrocatalysts. *J Mater Chem A*. 2015;3:18372-9.

[21] Burke MS, Kast MG, Trotochaud L, Smith AM, Boettcher SW. Cobalt-iron (oxy)hydroxide oxygen evolution electrocatalysts: the role of structure and composition on activity, stability, and mechanism. *J Am Chem Soc*. 2015;137:3638-48.

[22] Wang Q, Xue X, Lei Y, Wang Y, Feng Y, Xiong X, et al. Engineering of Electronic States on  $\text{Co}_3\text{O}_4$  Ultrathin Nanosheets by Cation Substitution and Anion Vacancies for Oxygen Evolution Reaction. *Small*. 2020;16:e2001571.

[23] Zhao Y, Zhang J, Wu W, Guo X, Xiong P, Liu H, et al. Cobalt-doped  $\text{MnO}_2$  ultrathin nanosheets with abundant oxygen vacancies supported on functionalized carbon nanofibers for efficient oxygen evolution. *Nano Energy*. 2018; 54: 129-137.

- [24] Song C, Liu Y, Wang Y, Tang S, Li W, Li Q, et al. Highly efficient oxygen evolution and stable water splitting by coupling NiFe LDH with metal phosphides. *Science China Materials*. 2021;64:1662-70.
- [25] Bandal HA, Jadhav AR, Chaugule AA, Chung W J, Kim H. Fe<sub>2</sub>O<sub>3</sub> hollow nanorods/CNT composites as an efficient electrocatalyst for oxygen evolution reaction. *Electrochimica Acta*. 2016; 222: 1316-1325.
- [26] Chen J, Wu X, Selloni A, Electronic structure and bonding properties of cobalt oxide in the spinel structure. *Physical Review B*. 2011; 83: 245204.
- [27] Wang D, Du Y, Wang X, Cuo Z, Chen Y. In-situ electro-deposition synthesis of MnO<sub>x</sub>-NiCo<sub>2</sub>O<sub>4</sub> monolithic catalyst with rich phase interfaces. *Chinese Chemical Letters*. 2021;32:21-4.
- [28] Yang X, Li H, Lu A-Y, Min S, Idriss Z, Hedhili MN, et al. Highly acid-durable carbon coated Co<sub>3</sub>O<sub>4</sub> nanoarrays as efficient oxygen evolution electrocatalysts. *Nano Energy*. 2016; 25: 42-50.
- [29] Friebel D, Louie MW, Bajdich M, Sanwald KE, Cai Y, Wise AM, et al. Identification of highly active Fe sites in (Ni,Fe)OOH for electrocatalytic water splitting. *J Am Chem Soc*. 2015;137:1305-13.
- [30] Asadizadeh S, Amirnasr M, Meghdadi S, Fadaei Tirani F, Schenk K. Facile synthesis of Co<sub>3</sub>O<sub>4</sub> nanoparticles from a novel tetranuclear cobalt(III) complex. Application as efficient electrocatalyst for oxygen evolution reaction in alkaline media. *International Journal of Hydrogen Energy*. 2018; 43: 4922-4931.
- [31] Du H, Li Y, Ding F, Zhao J, Zhang X, Li Y, et al. Boosting the capacitance of NiCo<sub>2</sub>O<sub>4</sub> hierarchical structures on nickel foam in supercapacitors. *International Journal of Hydrogen Energy*. 2018; 43: 15348-15357.
- [32] Hsu CS, Suen NT, Hsu YY, Lin HY, Tung CW, Liao YF, et al. Valence- and element-dependent water oxidation behaviors: in situ X-ray diffraction, absorption and electrochemical impedance spectroscopies. *Physical chemistry chemical physics : PCCP*. 2017;19:8681-93.
- [33] Ren Q-Q, Yu F-D, Zhang S-W, Yin B-S, Wang Z-B, Ke K. Enhanced electrochemical performance by size-dependent SEI layer reactivation of NiCo<sub>2</sub>O<sub>4</sub> anodes for lithium ion batteries. *Electrochimica Acta*. 2019; 297: 1011-1017.
- [34] Liu W, Bao J, Xu L, Guan M, Wang Z, Qiu J, Huang Y, et al. NiCo<sub>2</sub>O<sub>4</sub> ultrathin nanosheets with oxygen vacancies as bifunctional electrocatalysts for Zn-air battery/ *Applied Surface Science*. 2019; 478: 552-559.
- [35] Zou L, Jiang Y, Cheng J, Chen Y, Chi B, Pu J, et al. Bifunctional catalyst of well-dispersed RuO<sub>2</sub> on NiCo<sub>2</sub>O<sub>4</sub> nanosheets as enhanced cathode for lithium-oxygen batteries. *Electrochimica Acta*. 2018; 262: 97-106.
- [36] Chen R, Wang H-Y, Miao J, Yang H, Liu B. A flexible high-performance oxygen evolution electrode with three-dimensional NiCo<sub>2</sub>O<sub>4</sub> core-shell nanowires, *Nano Energy*, 2015; 11:: 333-340.
- [37] Liu Y, Du Y, Gao W-K, Dong B, Han Y, Wang L. Surface phosphorsulfurization of NiCo<sub>2</sub>O<sub>4</sub> nanoneedles supported on carbon cloth with enhanced electrocatalytic activity for hydrogen evolution, *Electrochimica Acta*. 2018; 290: 339-346.

- [38] Zhang H, Li H, Wang H, He K, Wang S, Tang Y, et al. NiCo<sub>2</sub>O<sub>4</sub>/N-doped graphene as an advanced electrocatalyst for oxygen reduction reaction, *Journal of Power Sources*. 2015; 280: 640-648.
- [39] Zhang L, Zhang D, Ren Z, Huo M, Dang G, Min F, et al. Mesoporous NiCo<sub>2</sub>O<sub>4</sub> Micro/nanospheres with Hierarchical Structures for Supercapacitors and Methanol Electro-oxidation. *ChemElectroChem*, 2017; 4: 441-449.
- [40] Zhang M, de Respinis M, Frei H. Time-resolved observations of water oxidation intermediates on a cobalt oxide nanoparticle catalyst. *Nature Chemistry*. 2014; 6: 362-367.
- [41] Xia B, Wang T, Jiang X, Li J, Zhang T, Xi P, et al. N<sup>+</sup>-ion irradiation engineering towards the efficient oxygen evolution reaction on NiO nanosheet arrays. *Journal of Materials Chemistry A*, 2019; 7: 4729-4733.
- [42] Wu L-K, Wu W-Y, Xia J, Cao H-Z, Hou G-Y, Tang Y-P, et al. Nanostructured NiCo@NiCoO<sub>x</sub> core-shell layer as efficient and robust electrocatalyst for oxygen evolution reaction. *Electrochimica Acta*. 2017; 254: 337-347.
- [43] Zhang B, Lui YH, Ni H, Hu S. Bimetallic (Fe<sub>x</sub>Ni<sub>1-x</sub>)<sub>2</sub>P nanoarrays as exceptionally efficient electrocatalysts for oxygen evolution in alkaline and neutral media, *Nano Energy*. 2017; 38: 553-560.
- [44] Gao Z-W, Liu J-Y, Chen X-M, Zheng X-L, Mao J, Liu H, et al. Engineering NiO/NiFe LDH Intersection to Bypass Scaling Relationship for Oxygen Evolution Reaction via Dynamic Tridimensional Adsorption of Intermediates. *Advanced Materials*. 2019; 31: 1804769.
- [45] Srinivasan R. Advances in Application of Natural Clay and Its Composites in Removal of Biological, Organic, and Inorganic Contaminants from Drinking Water. *Advances in Materials Science and Engineering*. 2011; 11: e872531.
- [46] Uddin MK. A review on the adsorption of heavy metals by clay minerals, with special focus on the past decade. *Chemical Engineering Journal*. 2017; 308: 438-462.
- [47] Maged A, Ismael IS, Kharbush S, Sarkar B, Peräniemi S, Bhatnagar A. Enhanced interlayer trapping of Pb(II) ions within kaolinite layers: intercalation, characterization, and sorption studies. *Environ Sci Pollut Res*. 2020; 27: 1870-1887.
- [48] Chang P-H, Li Z, Jiang W-T, Jean J-S. Adsorption and intercalation of tetracycline by swelling clay minerals. *Applied Clay Science*. 2009; 46: 27-36.
- [49] Peng K, Fu L, Ouyang J, Yang H. Emerging Parallel Dual 2D Composites: Natural Clay Mineral Hybridizing MoS<sub>2</sub> and Interfacial Structure. *Advanced Functional Materials*. 2016; 26: 2666-2675.
- [50] Shahwan T, Üzümlü Ç, Eroğlu A E, Lieberwirth I. Synthesis and characterization of bentonite/iron nanoparticles and their application as adsorbent of cobalt ions, *Applied Clay Science*, 2010;47: 257-262.
- [51] Fu L, Yan Z, Zhao Q, Yang H. Novel 2D Nanosheets with Potential Applications in Heavy Metal Purification: A Review. *Advanced Materials Interfaces*. 2018; 5: 1801094.

- [52] Chelgani SC, Rudolph M, Kratzsch R, Sandmann D, Gutzmer J. A Review of Graphite Beneficiation Techniques. *Mineral Processing and Extractive Metallurgy Review*. 2016; 37: 58-68.
- [53] Alipour E, Majidi MR, Saadatirad A, Golabi SM, Alizadeh A M. Simultaneous determination of dopamine and uric acid in biological samples on the pretreated pencil graphite electrode. *Electrochimica Acta*. 2013; 91: 36-42.
- [54] Gong ZQ, Sujari ANA, Ab Ghani S. Electrochemical fabrication, characterization and application of carboxylic multi-walled carbon nanotube modified composite pencil graphite electrodes. *Electrochimica Acta*. 2012; 65: 257-265.
- [55] Kariuki JK. An Electrochemical and Spectroscopic Characterization of Pencil Graphite Electrodes. *Journal of The Electrochemical Society*. 2012;159: H747.
- [56] Tavares PHCP, Barbeira PJS. Manganese oxide-based materials as electrochemical supercapacitor electrodes. *J Appl Electrochem*. 2008; 38: 827-832.
- [57] Lu X, Zhao C. Electrodeposition of hierarchically structured three-dimensional nickel-iron electrodes for efficient oxygen evolution at high current densities. *Nature Communications*, 2015; 6: 6616.
- [58] Aoki K, Okamoto T, Kaneko H, Nozaki K, Negishi A. Applicability of graphite reinforcement carbon used as the lead of a mechanical pencil to voltammetric electrodes. *Journal of Electroanalytical Chemistry and Interfacial Electrochemistry*. 1989; 263: 323-331.
- [59] Kariuki J, Ervin E, Olafson C. Development of a Novel, Low-Cost, Disposable Wooden Pencil Graphite Electrode for Use in the Determination of Antioxidants and Other Biological Compounds. *Sensors (Basel)*. 2015;15: 18887-18900.
- [60] Jiang J, Sun F, Zhou S, Hu W, Zhang H, Dong J, et al. Atomic-level insight into super-efficient electrocatalytic oxygen evolution on iron and vanadium co-doped nickel (oxy)hydroxide. *Nature Communications*. 2018; 9: 2885.
- [61] Yang H, Gong L, Wang H, Dong C, Wang J, Qi K, et al. Preparation of nickel-iron hydroxides by microorganism corrosion for efficient oxygen evolution. *Nature Communications*. 2020; 11: 5075.
- [62] Su X, Wang Y, Zhou J, Gu S, Li J, Zhang S. Operando Spectroscopic Identification of Active Sites in NiFe Prussian Blue Analogues as Electrocatalysts: Activation of Oxygen Atoms for Oxygen Evolution Reaction. *J. Am. Chem. Soc*. 2018;140: 11286-11292.
- [63] Fu Q, Wu T, Fu G, Gao T, Han J, Yao T, Zhang Y, et al. Skutterudite-Type Ternary Co<sub>1-x</sub>Ni<sub>x</sub>P<sub>3</sub> Nanoneedle Array Electrocatalysts for Enhanced Hydrogen and Oxygen Evolution. *ACS Energy Letters*. 2018; 3: 1744-1752.
- [64] Guan C, Xiao W, Wu H, Liu X, Zang W, Zhang H, et al. Hollow Mo-doped CoP nanoarrays for efficient overall water splitting. *Nano Energy*. 2018; 48: 73-80.
- [65] Li J, Wei G, Zhu Y, Xi Y, Pan X, Ji Y, Zatonovsky IV, et al. Hierarchical NiCoP nanocone arrays supported on Ni foam as an efficient and stable bifunctional electrocatalyst for overall water splitting. *Journal of Materials Chemistry A*. 2017;5: (), 14828-14837.

- [66] Wang J, Gan L, Zhang W, Peng Y, Yu H, Yan Q, et al. In situ formation of molecular Ni-Fe active sites on heteroatom-doped graphene as a heterogeneous electrocatalyst toward oxygen evolution. *Science Advances*. 2018; 4: eaap7970.
- [67] Li H, Chen S, Zhang Y, Zhang Q, Jia X, Zhang Q, et al. Systematic design of superaerophobic nanotube-array electrode comprised of transition-metal sulfides for overall water splitting. *Nature Communications*. 2018; 9: 2452.
- [68] Lin J, Wang P, Wang H, Li C, X. Si, Qi J, Cao J, Zhong Z, et al. Defect-Rich Heterogeneous MoS<sub>2</sub>/NiS<sub>2</sub> Nanosheets Electrocatalysts for Efficient Overall Water Splitting. *Advanced Science*. 2019; 6: 1900246.
- [69] Tian J, Chen J, Liu J, Tian Q, Chen P. Graphene quantum dot engineered nickel-cobalt phosphide as highly efficient bifunctional catalyst for overall water splitting. *Nano Energy*. 2018;48: 284-291.
- [70] Gnanasekaran L, Hemamalini R, Saravanan R, Ravichandran K, Gracia F, Agarwal S, et al. Synthesis and characterization of metal oxides (CeO<sub>2</sub>, CuO, NiO, Mn<sub>3</sub>O<sub>4</sub>, SnO<sub>2</sub> and ZnO) nanoparticles as photo catalysts for degradation of textile dyes. *Journal of Photochemistry and Photobiology B: Biology*. 2017;173: 43-49.
- [71] Silva VD, Simões TA, Grilo JPF, Medeiros ES, Macedo DA. Impact of the NiO nanostructure morphology on the oxygen evolution reaction catalysis. *Journal of Materials Science*. 2020; 55: 6648-6659.
- [72] Peck MA, Langell MA. Comparison of Nanoscaled and Bulk NiO Structural and Environmental Characteristics by XRD, XAFS, and XPS. *Chem. Mater*. 2012; 24: 4483-4490.
- [73] Biesinger MC, Payne BP, Grosvenor AP, Lau L W M, Gerson AR, Smart R S C. Resolving surface chemical states in XPS analysis of first row transition metals, oxides and hydroxides: Cr, Mn, Fe, Co and Ni. *Applied Surface Science*. 2011; 257: 2717-2730.
- [74] Kim K S, Davis R E. Electron spectroscopy of the nickel-oxygen system. *Journal of Electron Spectroscopy and Related Phenomena*. 1972; 1: 251-258.
- [75] Kim K S, Winograd N. X-ray photoelectron spectroscopic studies of nickel-oxygen surfaces using oxygen and argon ion-bombardment. *Surface Science*. 1974; 43: 625-643.
- [76] Zhang S-Y, Li T-T, Zhu H-L, Zheng Y-Q. Co<sub>3</sub>O<sub>4</sub> polyhedrons with enhanced electric conductivity as efficient water oxidation electrocatalysts in alkaline medium. *Journal of Materials Science*. 2018; 53: 4323-4333.
- [77] Veeramani V, Madhu R, Chen S-M, Sivakumar M, Hung C-T, N Miyamoto C-T, et al. NiCo<sub>2</sub>O<sub>4</sub>-decorated porous carbon nanosheets for high-performance supercapacitors. *Electrochimica Acta*. 2017; 247: 288-295.
- [78] Marco J F, Gancedo J R, Gracia M, Gautier J L, Ríos E, Berry F J. Characterization of the Nickel Cobaltite, NiCo<sub>2</sub>O<sub>4</sub>, Prepared by Several Methods: An XRD, XANES, EXAFS, and XPS Study. *Journal of Solid State Chemistry*. 2000;153: 74-81.
- [79] Wang W, Chu Q, Zhang Y, Zhu W, Wang X, Liu X. Nickel foam supported mesoporous NiCo<sub>2</sub>O<sub>4</sub> arrays with excellent methanol electro-oxidation performance. *New J. Chem*. 2015; 39: 6491-6497.

- [80] Kim J G, Pugmire D L, Battaglia D, Langell M A. Analysis of the NiCo<sub>2</sub>O<sub>4</sub> spinel surface with Auger and X-ray photoelectron spectroscopy. *Applied Surface Science*. 2000; 165: 70-84.
- [81] Sinha P, Datar A, Jeong C, Deng X, Chung Y G, Lin L-C. Exploring the Potential of Defective UiO-66 as Reverse Osmosis Membranes for Desalination. *The Journal of Physical Chemistry C*. 2019; 123: 20195-20209.
- [82] Sun Q, Diao K, Sun T, Li M, Cui X, Tian H, Xiang B. Enhanced gas-sensing performance of SnO<sub>2</sub>/Nb<sub>2</sub>O<sub>5</sub> hybrid nanowires. *RSC Advances*. 2016; 6: 105317-105321.
- [83] Han Y, Qi P, Li S, Feng X, Zhou J, Li H, et al. A novel anode material derived from organic-coated ZIF-8 nanocomposites with high performance in lithium ion batteries. *Chemical Communications*. 2014; 50: 8057-8060.
- [84] Walton K S, Snurr R Q. Applicability of the BET Method for Determining Surface Areas of Microporous Metal–Organic Frameworks. *J. Am. Chem. Soc.* 2007; 129: 8552-8556.
- [85] He X, Yin F, Li G. A Co/metal–organic-framework bifunctional electrocatalyst: The effect of the surface cobalt oxidation state on oxygen evolution/reduction reactions in an alkaline electrolyte. *International Journal of Hydrogen Energ.*, 2015; 40: 9713-9722.
- [86] Lu Z, Wang H, Kong D, Yan K, Hsu P-C, Zheng G, et al. Electrochemical tuning of layered lithium transition metal oxides for improvement of oxygen evolution reaction. *Nature Communications*. 2014; 5: 4345.
- [87] Gholivand M B, Khodadadian M, Bahrami G. Molecularly Imprinted Polymer Preconcentration and Flow Injection Amperometric Determination of 4-Nitrophenol in Water. *Analytical Letters*. 2015; 48: 2856-2869.
- [88] Akanda M R, Sohail M, Aziz M A, Kawde A-N. Recent Advances in Nanomaterial-Modified Pencil Graphite Electrodes for Electroanalysis. *Electroanalysis*. 2016; 28: 408-424.
- [89] Wu L-K, Liu X-Y, Hu J-M. Electrodeposited SiO<sub>2</sub> film: a promising interlayer of a highly active Ti electrode for the oxygen evolution reaction. *Journal of Materials Chemistry A*. 2016; 4: 11949-11956.
- [90] He X, Tan J, Wei J, Yin F, Chen B, Liang X, et al. MgO-Co/N-doped carbon with inactive MgO enhancing electrocatalytic activity toward oxygen evolution and reduction reactions. *Applied Surface Science*. 2020; 508: 144758.
- [91] Xu W, Lyu F, Bai Y, Gao A, Feng J, Cai Z, et al. Porous cobalt oxide nanoplates enriched with oxygen vacancies for oxygen evolution reaction. *Nano Energy*. 2018; 43: 110-116.
- [92] Zhang J-J, Wang H-H, Zhao T-J, Zhang K-X, Wei X, Jiang Z-D, et al. Oxygen Vacancy Engineering of Co<sub>3</sub>O<sub>4</sub> Nanocrystals through Coupling with Metal Support for Water Oxidation. *ChemSusChem*. 2017; 10: 2875-2879.
- [93] Guo Y, Park T, Yi J W, Henzie J, Kim J, Wang Z, et al. Nanoarchitectonics for Transition-Metal-Sulfide-Based Electrocatalysts for Water Splitting. *Advanced Materials*. 2019; 31: 1807134.
- [94] Joo J, Kim T, Lee J, Choi S-I, Lee K. Morphology-Controlled Metal Sulfides and Phosphides for Electrochemical Water Splitting. *Advanced Materials*. 2019; 31: 1806682.

- [95] He X., Tan J., Wei J., Yin F., Chen B., Liang X., Li G., 2020. MgO-Co/N-doped carbon with inactive MgO enhancing electrocatalytic activity toward oxygen evolution and reduction reactions. *Appl. Surf. Sci.* 508:144758.
- [96] Li X, Hao X, Abudula A, Guan G. Nanostructured catalysts for electrochemical water splitting: current state and prospects. *Journal of Materials Chemistry A.* 2016; 4: 11973-12000.
- [97] Song F, Bai L, Moysiadou A, Lee S, Hu C, Liardet L, et al. Transition Metal Oxides as Electrocatalysts for the Oxygen Evolution Reaction in Alkaline Solutions: An Application-Inspired Renaissance. *J. Am. Chem. Soc.* 2018; 140: 7748-7759.
- [98] Matsumoto Y, Sato E. Electrocatalytic properties of transition metal oxides for oxygen evolution reaction. *Materials Chemistry and Physics.* 1986; 14: 397-426.
- [99] Fabbri E, Habereder A, Waltar K, Kötzer R, Schmidt T J. Developments and perspectives of oxide-based catalysts for the oxygen evolution reaction. *Catal. Sci. Technol.* 2014; 4: 3800-3821.
- [100] Trotochaud L, Young S L, Ranney J K, Boettcher S W. Nickel-Iron Oxyhydroxide Oxygen-Evolution Electrocatalysts: The Role of Intentional and Incidental Iron Incorporation. *J. Am. Chem. Soc.* 2014; 136: 6744-6753.
- [101] Scrivener KL, Füllmann T, Gallucci E, Walenta G, Bermejo E. Quantitative study of Portland cement hydration by X-ray diffraction/Rietveld analysis and independent methods. *Cement Concr Res* 2004;34:1541-7
- [102] Rendtorf NM, Conconi MS, Aglietti EF, Chain CY, Pasquevich AF, et al. Phase quantification of mullite/zirconia and zircon commercial powders using PAC and XRD techniques. *Hyperfine Interact* 2010;198:211-8
- [103] Corrigan D A. The Catalysis of the Oxygen Evolution Reaction by Iron Impurities in Thin Film Nickel Oxide Electrodes. *Journal of The Electrochemical Society.* 1987; 134: 377.
- [104] Chung D Y, Lopes P P, Martins P F B D, He H, Kawaguchi T, Zapol P, et al. Dynamic stability of active sites in hydr(oxy)oxides for the oxygen evolution reaction. *Nature Energy.* 2020; 5: 222-230.

### Figure Captions

**Figure 1** The comparison of  $\text{Co}_3\text{O}_4$  and  $\text{NiCo}_2\text{O}_4\text{-P}$  in terms of overpotential with already well-established electrocatalysts for OER at  $100 \text{ mA cm}^{-2}$  in 1M KOH aqueous solution (P stands for PGR).

**Figure 2** Powder XRD patterns of bare PGR,  $\text{NiCo}_2\text{O}_4\text{-P}$ ,  $\text{Co}_3\text{O}_4\text{-P}$ , and  $\text{NiO-P}$  (P stands for PGR).

**Figure 3** SEM images taken at different magnifications of the catalysts after their growth on PGR: a) and b) NiO-P, c) and d) Co<sub>3</sub>O<sub>4</sub>-P and e) and f) NiCo<sub>2</sub>O<sub>4</sub>-P (P stands for PGR).

**Figure 4** XPS spectra (a) Ni 2p<sub>3/2</sub> and (b) O 1s of NiO-P; (c) Co 2p<sub>3/2</sub> and (d) O 1s of Co<sub>3</sub>O<sub>4</sub>-P; (e) Ni 2p<sub>3/2</sub>, (f) Co 2p<sub>3/2</sub> and (g) O 1s of NiCo<sub>2</sub>O<sub>4</sub>-P (P stands for PGR).

**Figure 5** HRTEM micrographs (a and g), zoom-in of the green square area (b and h) (insert: corresponding Fast Fourier Transform (FFT)), TEM micrographs at low magnification (c and i) and corresponding EELS elemental maps of cobalt (d and j), nickel (e and k) and oxygen (f and l) of NiCo<sub>2</sub>O<sub>4</sub>-P before (a-f) and after the OER reactions (g-l) (P stands for PGR).

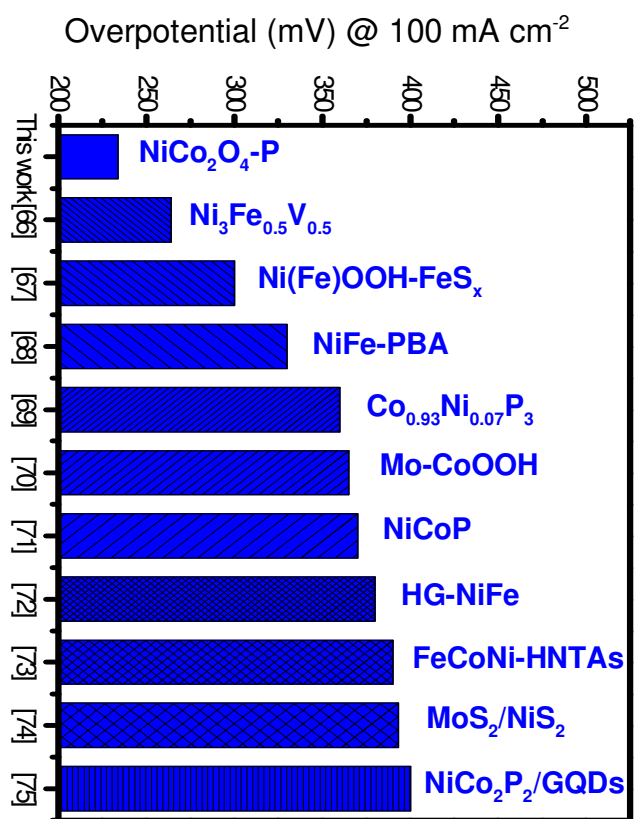
**Figure 6** BET analysis of a. bare graphite pencil, b. NiO-P, c. Co<sub>3</sub>O<sub>4</sub>-P, and d. NiCo<sub>2</sub>O<sub>4</sub>-P (inset shows the pore size distribution) (P stands for PGR).

**Figure 7** a. LSV curves of bare graphite pencil, NiO-P, Co<sub>3</sub>O<sub>4</sub>-P, NiCo<sub>2</sub>O<sub>4</sub>-P, 20%wt RuO<sub>2</sub>/C at a scan rate of 5mVs<sup>-1</sup> in 1.0M KOH at 25 °C, b. Plot of overpotential @ 100 mAcm<sup>-2</sup> versus bare graphite pencil, NiO-P, Co<sub>3</sub>O<sub>4</sub>-P, NiCo<sub>2</sub>O<sub>4</sub>-P, , c. Tafel plots in 1.0M KOH, d. Linear plot of current density versus different scan rates, e. multi-step chronoamperometry measurement in 1.0M KOH beginning from @ 100 mAcm<sup>-2</sup> for the time interval of 500 s and with consecutive rise of @50 mAcm<sup>-2</sup>, f. Multistep potential chronopotentiometric curve of NiO-P, Co<sub>3</sub>O<sub>4</sub>-P, NiCo<sub>2</sub>O<sub>4</sub>-P in 1.0M KOH at the beginning of 1.48 V vs RHE during each step and time interval of 500 s, g. Nyquist plots of bare graphite pencil, NiO-P, Co<sub>3</sub>O<sub>4</sub>-P, NiCo<sub>2</sub>O<sub>4</sub>-P in 1.0M KOH, inset showing the fitted equivalent circuit model (P stands for PGR).

**Figure 8** a. LSV curves of NiO-P before and after the durability test at a scan rate of 5mVs<sup>-1</sup> in 1.0 M KOH at 25 °C, b. LSV curves of Co<sub>3</sub>O<sub>4</sub>-P before and after the durability test at a scan rate of 5mVs<sup>-1</sup> in 1.0 M KOH, c. a. LSV curves of NiCo<sub>2</sub>O<sub>4</sub>-P before and after the durability test at a scan rate of 5mVs<sup>-1</sup> in 1.0 M KOH, d. chronoamperometric response of NiO-P in 1.0M KOH @ 100 mAcm<sup>-2</sup>, e. chronoamperometric response of Co<sub>3</sub>O<sub>4</sub>-P in 1.0M KOH @ 100 mAcm<sup>-2</sup>, f. chronoamperometric response of NiCo<sub>2</sub>O<sub>4</sub>-P in 1.0M KOH @ 100 mAcm<sup>-2</sup> (P stands for PGR).

**Figure 9** a. LSV curves of bare graphite pencil, NiO-P, Co<sub>3</sub>O<sub>4</sub>-P, NiCo<sub>2</sub>O<sub>4</sub>-P, at a scan rate of 5mVs<sup>-1</sup> in 6.0M KOH at 25 °C, b. LSV curves of Co<sub>3</sub>O<sub>4</sub>-P at a scan rate of 5mVs<sup>-1</sup> in 6.0M KOH at 25 °C and 60 °C, c. LSV curves NiCo<sub>2</sub>O<sub>4</sub>-P at a scan rate of 5mVs<sup>-1</sup> in 6.0M KOH at 25 °C and 60 °C, d. LSV curves of NiO-P at a scan rate of 5mVs<sup>-1</sup> in 6.0M KOH at 25 °C and 60 °C, e. Multistep current chronoamperometric response of NiO-P, Co<sub>3</sub>O<sub>4</sub>-P, NiCo<sub>2</sub>O<sub>4</sub>-P in 6.0M KOH at the beginning of 150 mAcm<sup>-2</sup> during each step and time interval of 500 s, f. Multistep potential chronopotentiometric curve of NiO-P, Co<sub>3</sub>O<sub>4</sub>-P, NiCo<sub>2</sub>O<sub>4</sub>-P in 6.0M KOH at the beginning of 1.48 V vs RHE during each step and time interval of 500 s (P stands for PGR).

Figure 1





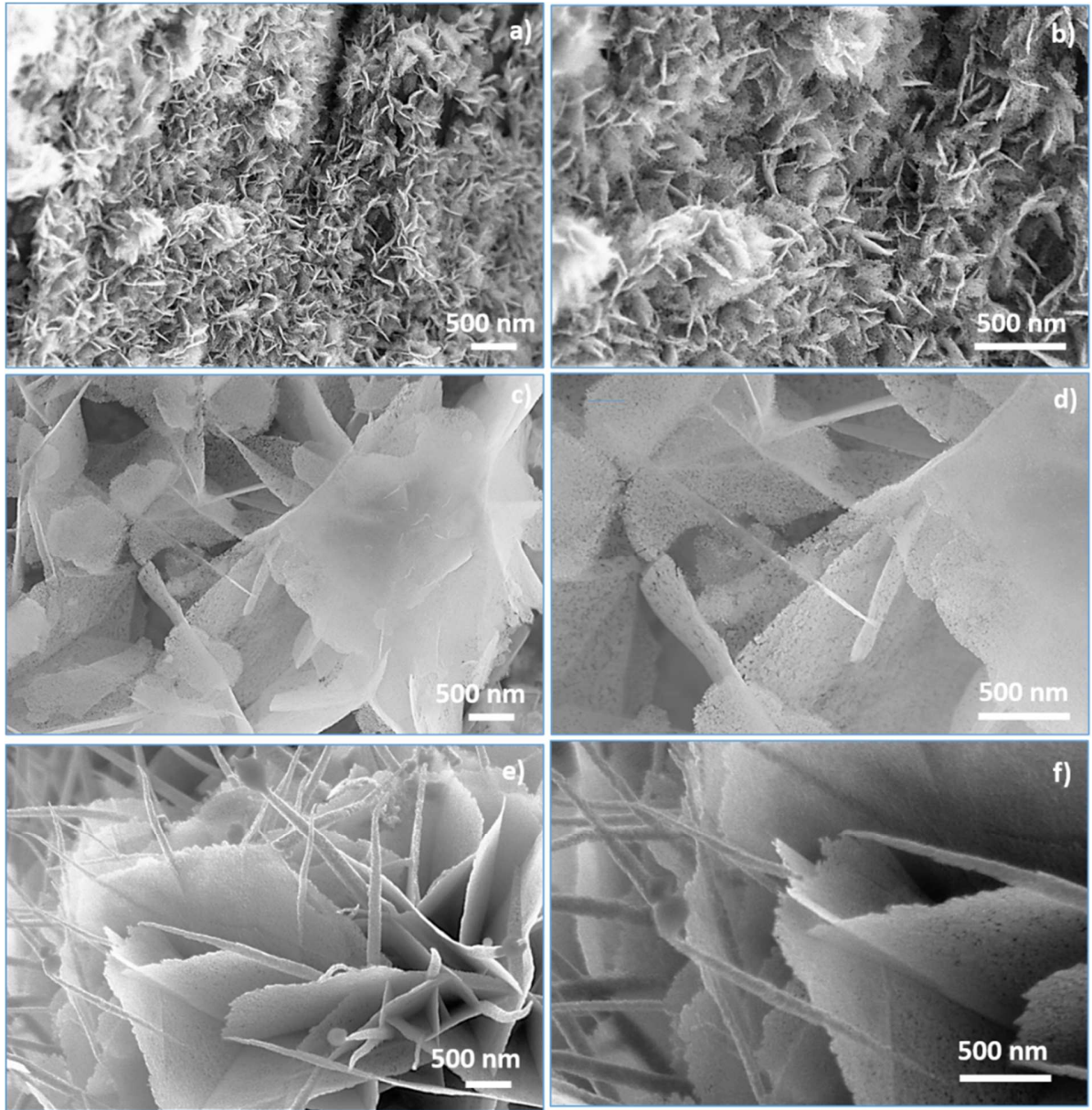
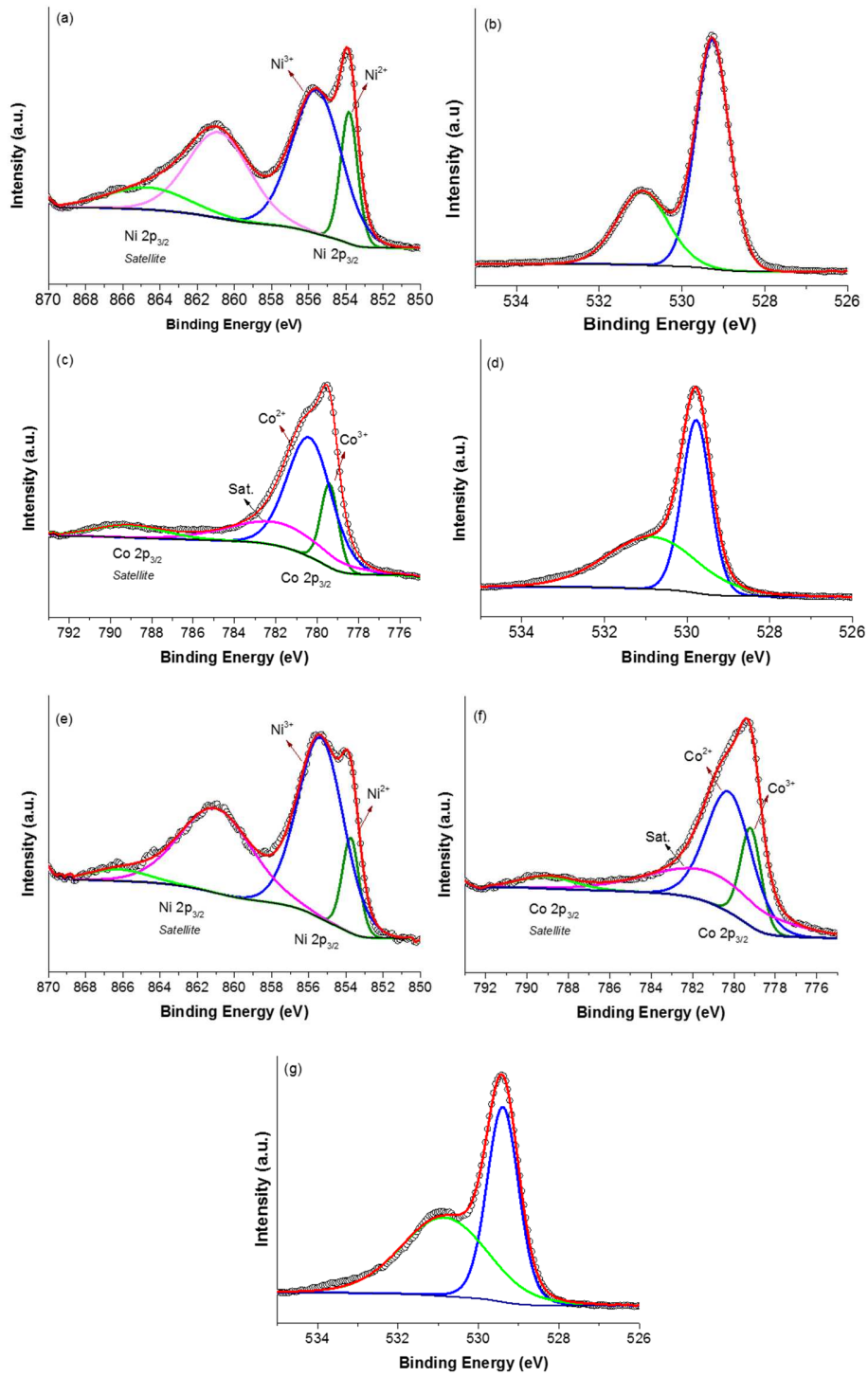


Figure 4



**Figure 5**

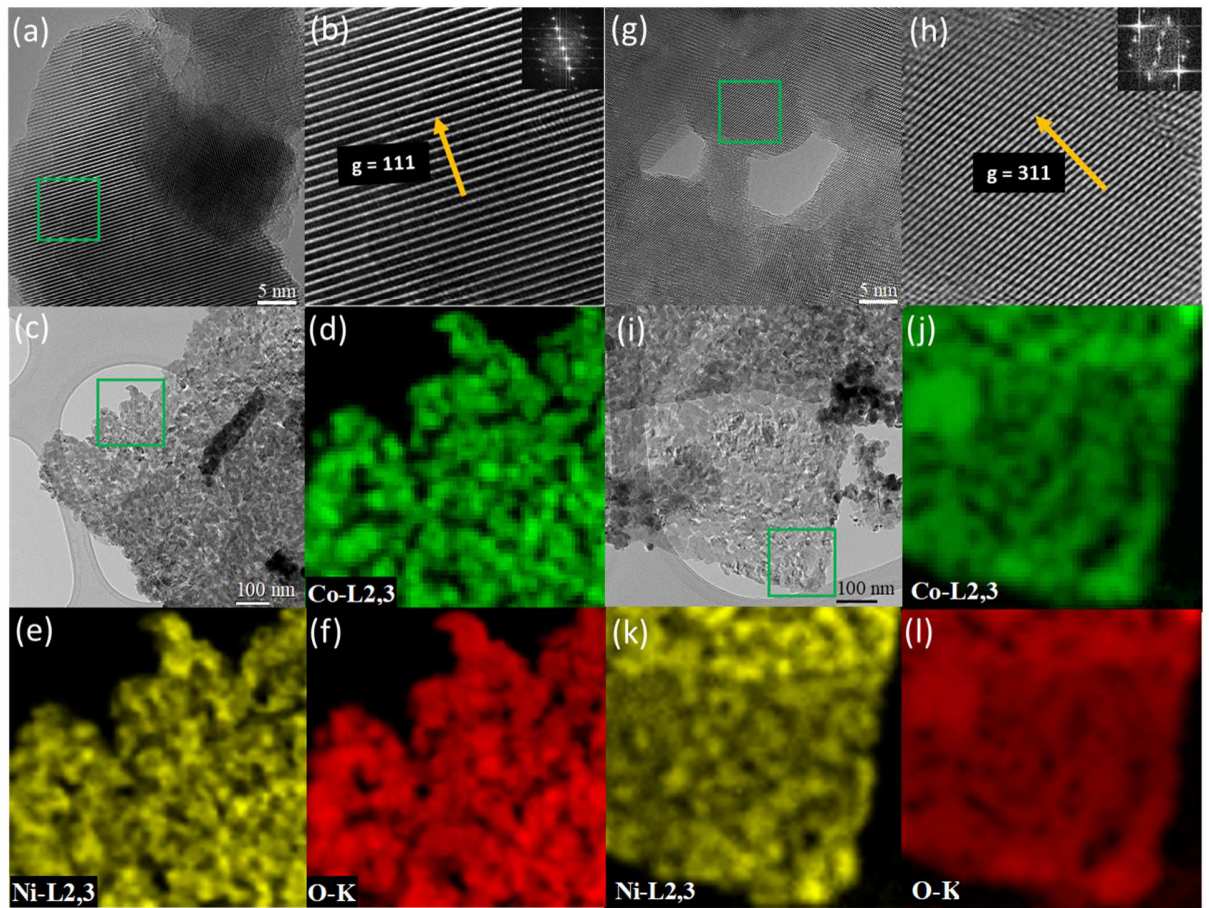
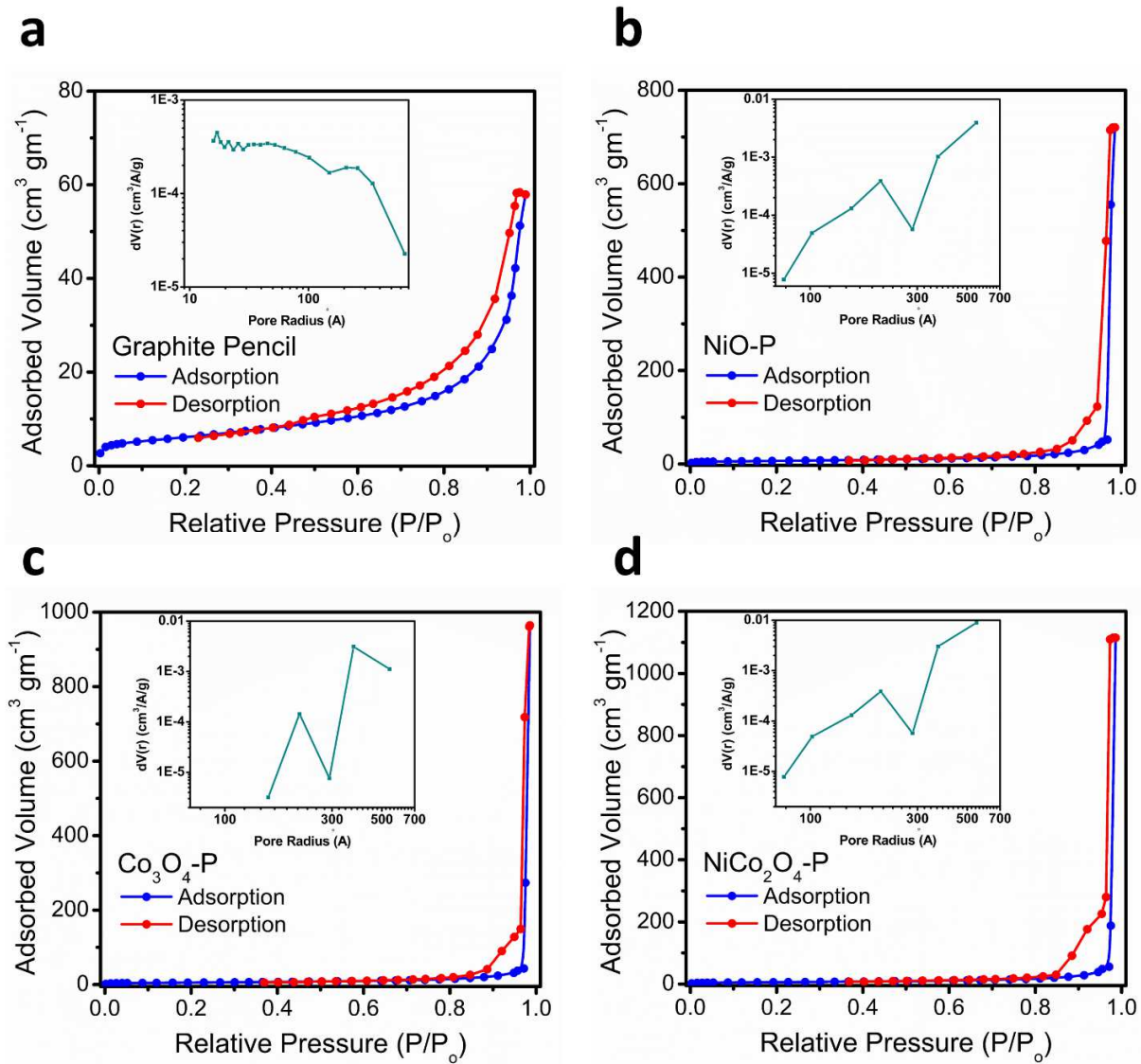
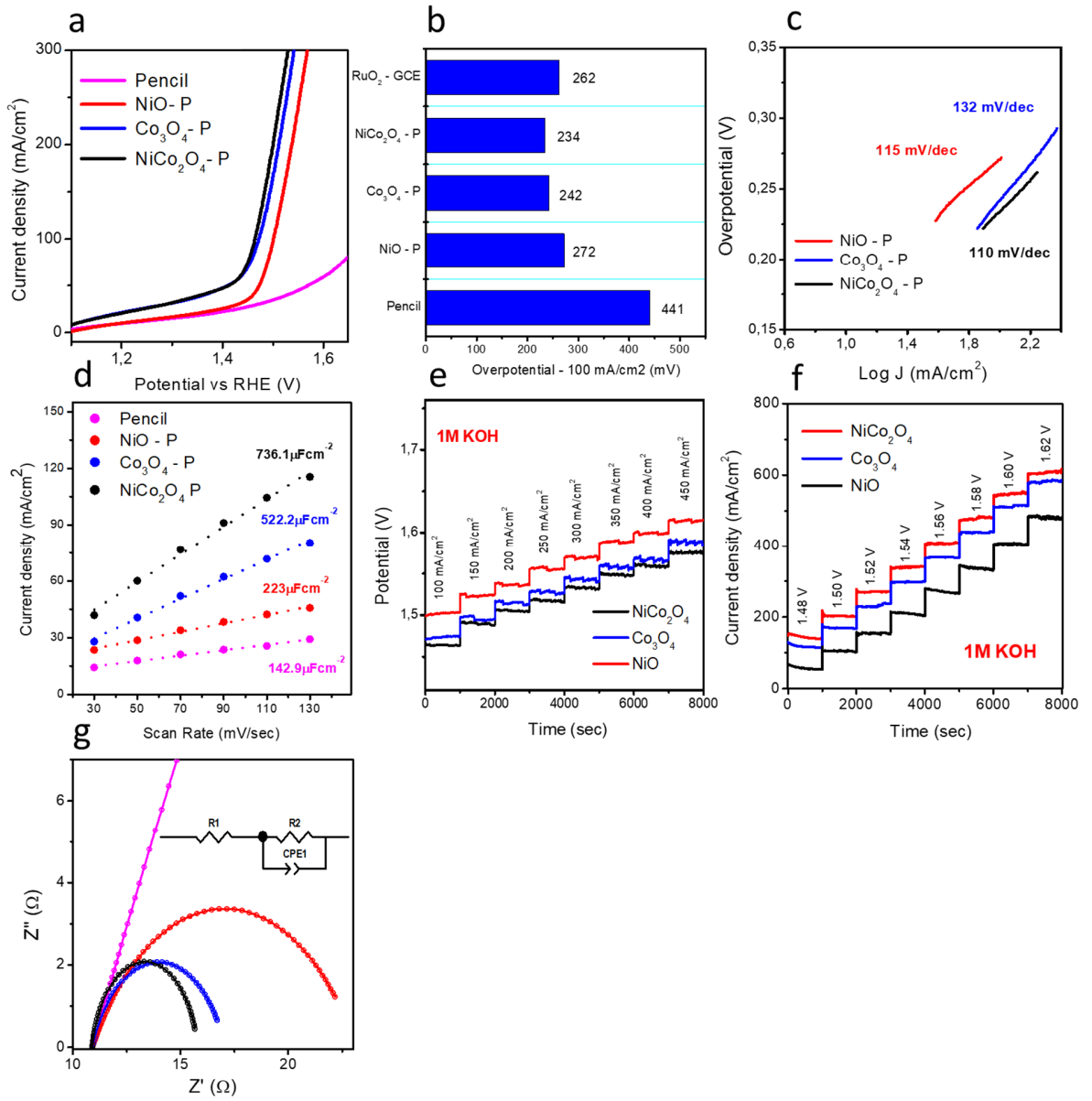


Figure 6



**Figure 7**



**Figure 8**

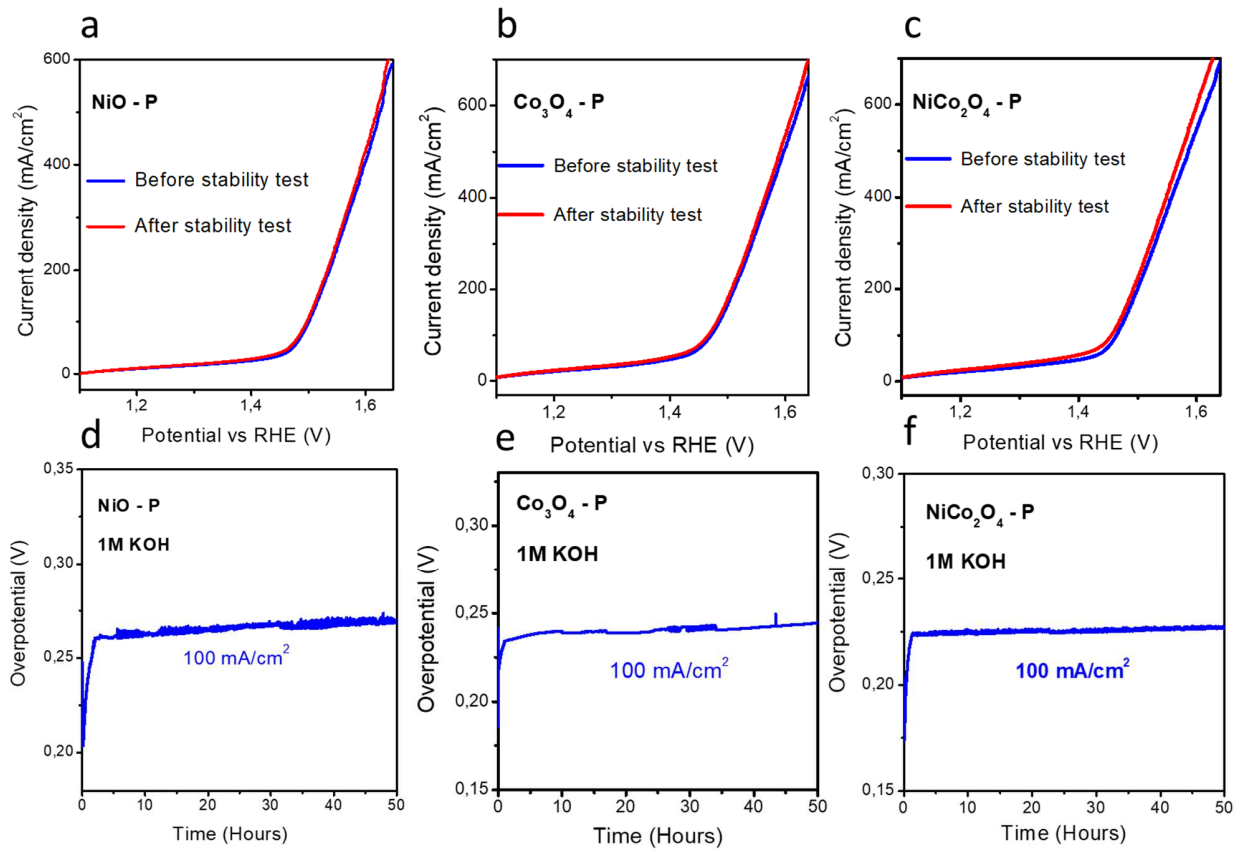
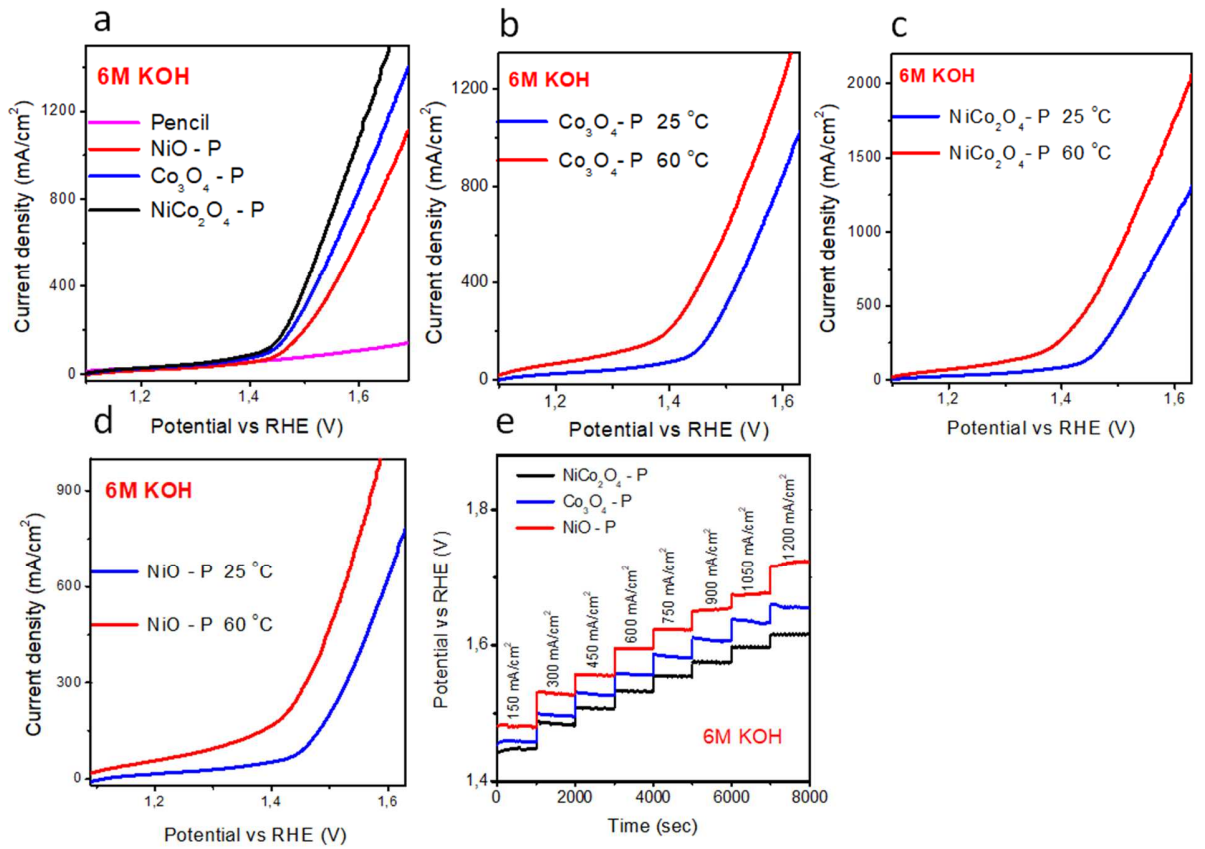


Figure 9



## Supplementary Information

### NiCo<sub>2</sub>O<sub>4</sub> nanostructures loaded onto pencil graphite rod: An advanced composite material for oxygen evolution reaction

Zafar Hussain Ibupoto<sup>a\*</sup>, Aneela Tahira<sup>a\*</sup>, Aqeel Ahmed Shah<sup>d</sup>, Umair aftar<sup>b</sup>, Muhammad Yameen Solangi<sup>b</sup>, Jaleel Ahmed Leghari<sup>b</sup>, Abdul Hanan Samoon<sup>b</sup>, Adeel Liaquat Bhatti<sup>c</sup>, Muhammad Ali Bhatti<sup>c</sup>, Raffaello Mazzaro<sup>f</sup>, Vittorio Morandi<sup>f</sup>, Muhammad Ishaq Abro<sup>b</sup>, Ayman Nafady<sup>g</sup>, Abdullah M Al-Enizi<sup>g</sup>, Mélanie Emo<sup>i</sup>, Brigitte Vigolo<sup>i\*</sup>

<sup>a</sup>Dr. M.A Kazi Institute of Chemistry University of Sindh Jamshoro, 76080, Sindh Pakistan

<sup>b</sup>Mehran University of Engineering and Technology, 7680 Jamshoro, Sindh Pakistan

<sup>c</sup>Institute of Physics University of Sindh Jamshoro, 76080, Sindh Pakistan

<sup>d</sup>NED University of Engineering and Technology Karachi, Sindh Pakistan

<sup>e</sup>Department of Environmental Sciences University of Sindh Jamshoro, 76080, Sindh Pakistan

<sup>f</sup>Institute for Microelectronics and Microsystems, Italian National Research Council, Section of Bologna, Via Piero Gobetti 101, 40129, Bologna, Italy

<sup>g</sup>Department of Chemistry, College of Science, King Saud University, Riyadh 11451, Saudi Arabia

<sup>i</sup>Université de Lorraine, CNRS, IJL, F-54000 Nancy, France

Corresponding authors: Zafar Hussian Ibupoto, PhD\*, Brigitte Vigolo, PhD, Aneela Tahira, PhD

Email address: zaffar.ibhupoto@usindh.edu.pk, brigitte.vigolo@univ-lorraine.fr

[aneelatahira80@gmail.com](mailto:aneelatahira80@gmail.com)

## S1. Materials and methods

**Materials.** The used chemicals include cobalt chloride hexahydrate, nickel chloride hexahydrate, potassium hydroxide, alumina slurry (0.05 $\mu$ m), ethanol 99.99%, and 5% Nafion membrane were

purchased from Sigma Aldrich Karachi, Pakistan. These chemicals were of analytical grade and used without any further purification. The Castell 9000 graphite pencil, 7B was made in Germany and purchased from a local market of Hyderabad, Sindh, Pakistan. The pencil graphite leads are composite materials consisting approximately (65% graphite, 30% clay 5% a binder (like wax, high polymer, or resins)). The desired solutions were prepared in the deionized water. The chemical composition of kaolinite (Kaol) is  $\text{Al}_2\text{Si}_2\text{O}_5(\text{OH})_4$  with distinctive 1:1 layered structure formed by the stacking of Al-O octahedral and Si-O tetrahedral geometry. The unique surface of kaolinite is consisting several hydroxyl groups, hydrophilic surface, high surface area, good stability and they play a vital role in catalytic processes. On other hand, bentonite is aluminum phyllosilicate clay and it mostly contains montmorillonite. The bentonite is inherited by Fe impurity in its chemical composition; therefore, it can play a vital role during water splitting.

**Synthesis of metal oxide nanostructures onto graphite pencil.** The wooden part of Castell 9000 graphite pencil, 7B was removed and naked graphite rod was cleaned with ethanol and washed several times with the deionized water. Then, graphite rod was dried at room temperature. For the growth of  $\text{Co}_3\text{O}_4$ , the precursor solution of 0.1 M cobalt chloride hexahydrate and 0.1 M urea was prepared in 100 mL of the deionized water. For the growth of NiO, the 0.1 M nickel chloride hexahydrate and 0.1 M urea was added to 100 mL of the deionized water. For the growth of  $\text{NiCo}_2\text{O}_4$ , the precursor solution of 0.1 M cobalt chloride hexahydrate and 0.1 M urea was prepared in 100 mL of the deionized water. Then 0.015 M nickel chloride hexahydrate was also added in this solution. Afterwards, cleaning the pencil graphite rods, they were vertically dipped in each precursor beaker and covered with the aluminum foil. Then growth solutions were kept at 95 °C for 5 h. After the completion of growth time, the graphite rods were coated with dense metal hydroxide nanostructures and washed several times with the deionized water. Then, they were annealed at 400 °C for 4 h in air to get metal oxide phase.

## **S2. Physical characterization of materials**

**Scanning Electron Microscopy and Energy Dispersive Spectroscopy.** SEM analysis is performed on a Zeiss LEO 1530 FE-SEM, operated at 5kV. The samples are directly observed as grown on the GPR substrate with an In-lens SE detector. EDS analysis is performed employing an Oxford 30 mm<sup>2</sup> SDD spectrometer, operating at 15kV. For XRD and XPS characterization, the

dense layer of NiCo<sub>2</sub>O<sub>4</sub>, Co<sub>3</sub>O<sub>4</sub>, and NiO nanostructures was removed from the graphite rod surface, collection both the graphite/clay mineral substrate and the produced metal oxide. **X-ray diffraction.** The crystallography of each material was investigated by the XRD (D8 Advance, Bruker) using CuK $\alpha$  radiation ( $\lambda= 1.54050 \text{ \AA}$ ), 45 mA, 45 kV and (2 $\theta$ ) scale range from 10 to 85°.at a scan rate of 1° min<sup>-1</sup>. Quantitative Rietveld analysis was used to quantify the relative distribution of each component in the composite system using HighScore Plus software [101, 102]. **X-ray photoelectron spectroscopy** spectra were collected on a Kratos Axis Ultra (Kratos Analytical, UK) spectrometer equipped with a monochromatic Al K $\alpha$  (1486.6 eV). All spectra were recorded at a 90° takeoff angle. The high-resolution regions were acquired with 0.1 eV step and 20 eV pass energy (instrumental resolution better than 0.5 eV). All binding energy values were charge corrected to the C 1s signal (284.6 eV). Curve fitting was performed using a combined Gaussian and Lorentzian line profile after Shirley's background subtraction by Casa XPS software. **Transmission electron microscopy** (TEM) observations were performed on a JEOL JEM ARM 200F-Cold FEG operating at 200 kV, equipped with spherical aberration (Cs) image and probe correctors. Electron energy loss spectroscopy (EELS) experiments were performed in scanning transmission electron microscopy (STEM) mode. The spectrometer was set to an energy dispersion of 0.25 eV/channel to collect O-K, Co-L<sub>2,3</sub> and Ni-L<sub>2,3</sub> edges. Supplementary X-maps were collected on an energy X-ray dispersive spectrometer (EDS) (JEOL Centurio). The oxide deposit was gently rubbed out of graphite rod before being deposited on a copper grid covered by a holey carbon film (200 mesh size).

**Electrochemical measurements.** In the typical three electrode assembly, a graphite rod and Ag/AgCl electrode filled with (3 M KCl) were used as the counter and references electrodes, respectively. The grown NiCo<sub>2</sub>O<sub>4</sub>, Co<sub>3</sub>O<sub>4</sub>, and NiO nanostructures onto graphite pencil rod and bare pencil rod were used as direct electrodes for the OER characterization. The grown metal oxide nanostructures onto the graphite rods were covered with 5% Nafion membrane as binder to avoid the leakage of the nanostructured materials from the surface of graphite rod during the measurements. Then pencil graphite rod was attached with copper wire through parafilm and also covered the most part of pencil graphite rod except a diameter of 0.12 cm<sup>2</sup> was exposed to electrolytic solution. After that, the pencil graphite rod electrode was placed into the electrochemical cell where its terminal was clamped with copper wire thus it complete the cell

circuit for the electrochemical analysis. The OER curves were measured at a scan rate of  $5 \text{ mVs}^{-1}$  using linear sweep voltammetry (LSV) in different electrolytic 0.1, 1.0, and 6.0 M solutions of KOH de-aerated by  $\text{N}_2$ . The purification of electrolyte (KOH) was ensured in order to avoid the effect of cation concentration on the electrochemical performance of working electrode by the reported method [103, 104]. The electrolyte purification was observed in a plastic cell in such a way the cell was remained untouched with the fluoropolymer material which could cause the contamination from the glassy parts of the cell. Prior to the LSV, cyclic voltammetry (CV) was used at a scan rate of  $10 \text{ mVs}^{-1}$  to stabilize the electrode. The cyclic voltammetry was used at different scan rates for the calculation of electrochemical active surface area. The electrochemical impedance spectroscopy was performed at the frequency range of 100 kHz to 0.1 Hz, sinusoidal potential of 5 mV and OER onset potential. All OER polarization curves are reported without iR compensation and the electrochemical experiments were performed on Versa-potentiostat made in Netherland. The measured experimental potentials are converted into reversible hydrogen electrode (RHE) using Nernst equation.

**Table S1:** The quantitative distribution of various components in each composite system using High score plus analysis on XRD data

	<b>SiO<sub>2</sub></b>	<b>Graphite</b>	<b>MgO</b>	<b>NiO</b>	<b>Co<sub>3</sub>O<sub>4</sub></b>	<b>NiCo<sub>2</sub>O<sub>4</sub></b>	<b>Total</b>
NiO-P	17.8	68.8	5.6	7.8	--	--	100
Co <sub>3</sub> O <sub>4</sub> -P	18.2	69.5	7.1	--	5.2	--	100
NiCo <sub>2</sub> O <sub>4</sub> -P	17.9	70.8	5.7	--	--	5.6	100
Pristine pencil graphite rod	18.9	73.8	7.3	--	--	--	100

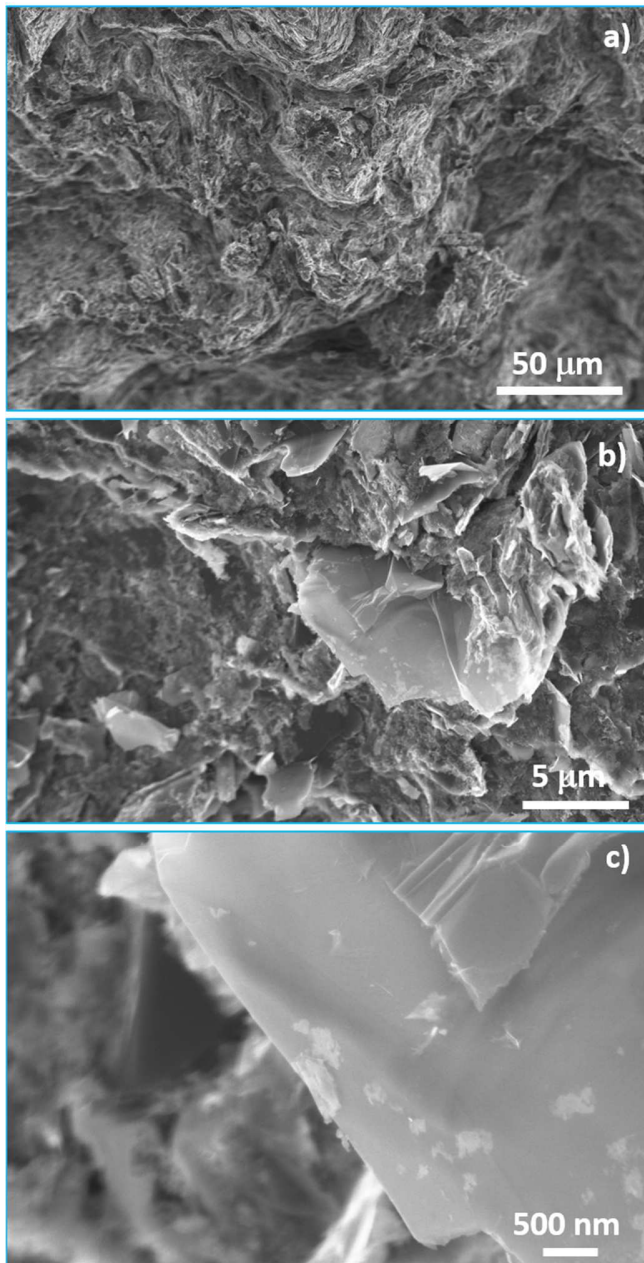


**Figure S1:** SEM images of PGR at different magnifications.

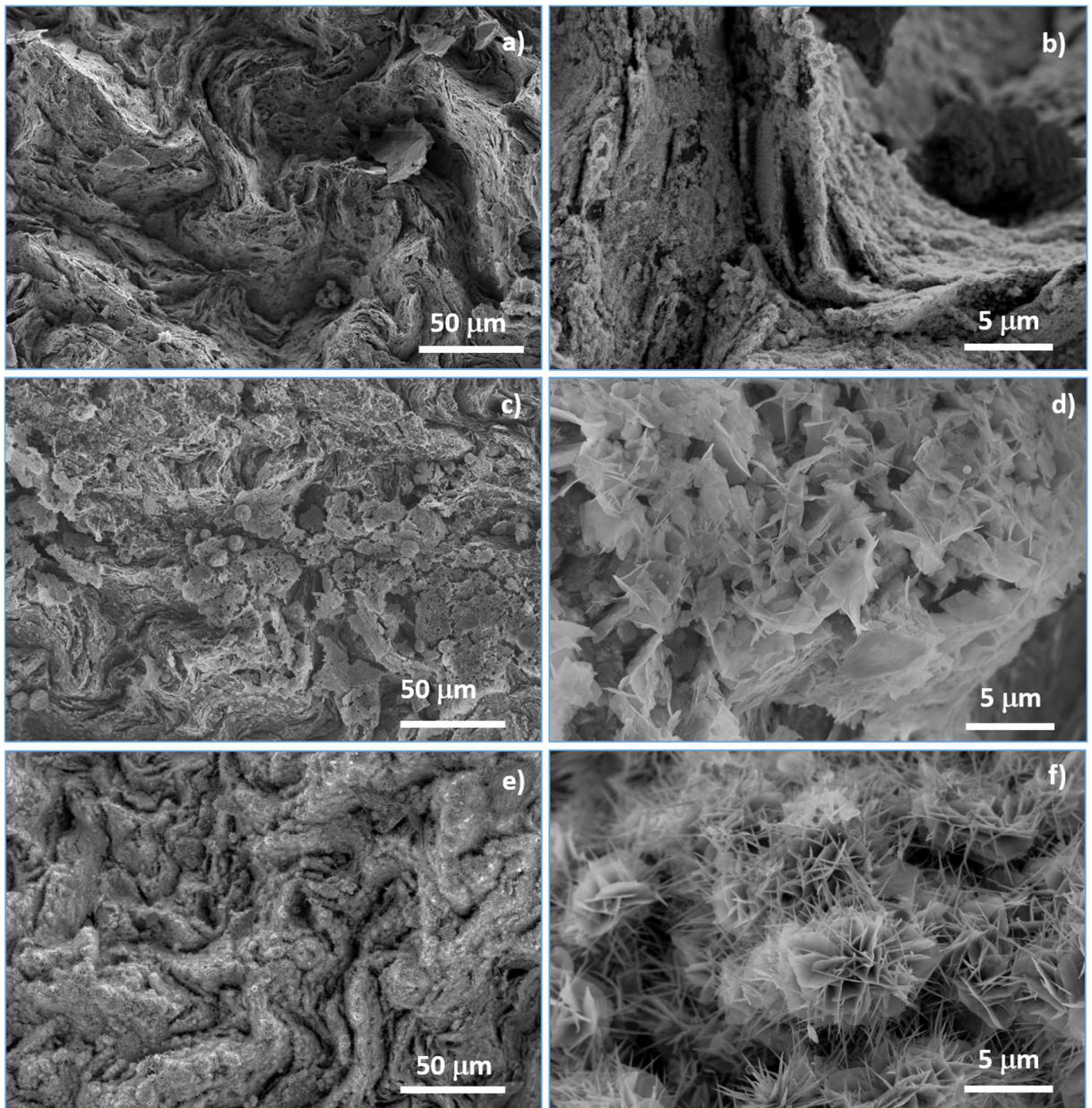


**Figure S2:** SEM images taken at different magnifications of the catalysts after their preparation: a) and b) NiO/PGR, c) and d)  $\text{Co}_3\text{O}_4$ /PGR and e) and f)  $\text{NiCo}_2\text{O}_4$ /PGR.

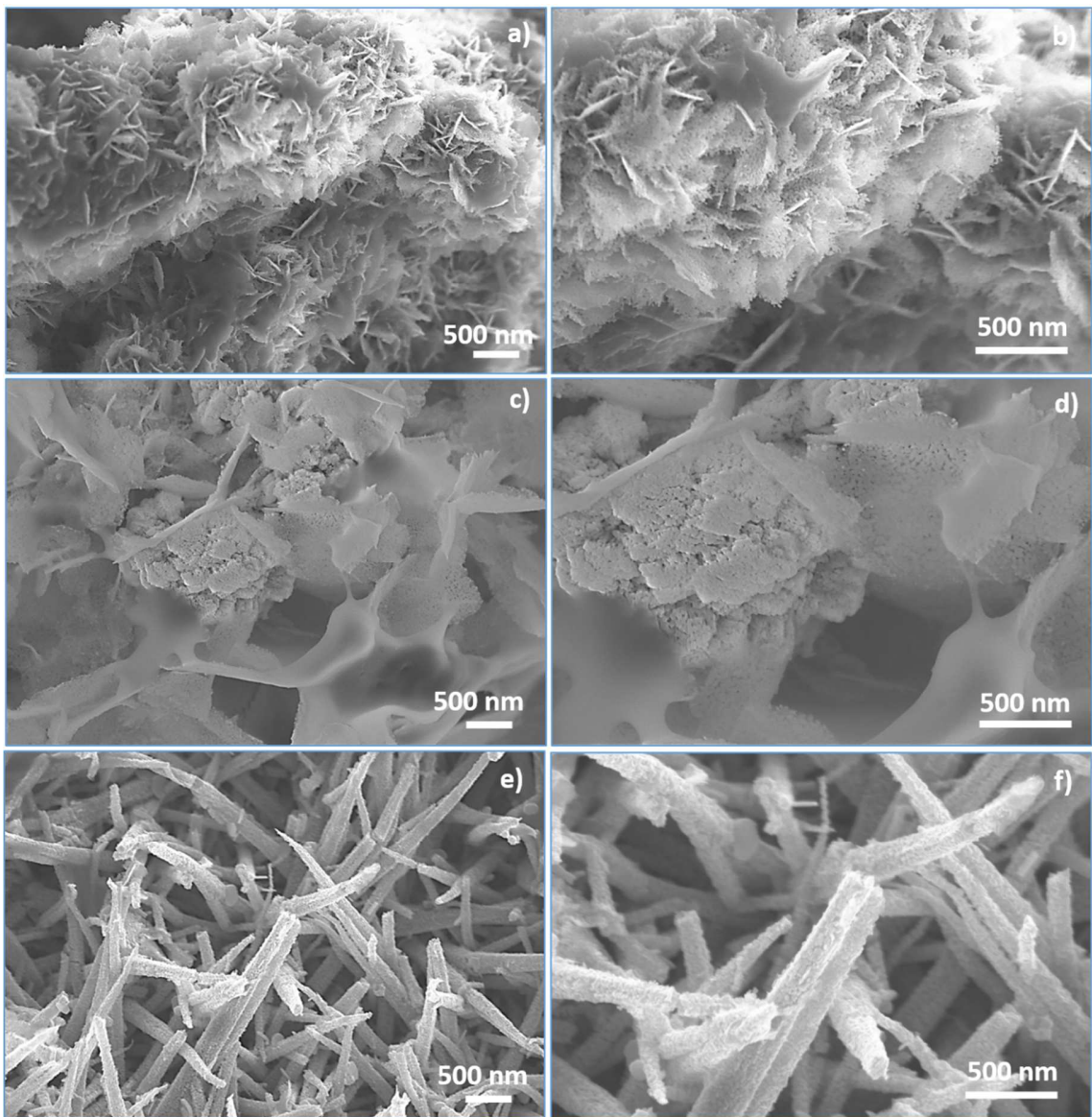


**Figure S3:** SEM images taken at different magnifications of the catalysts after OER experiments: a) and b) NiO/PGR, c) and d) Co<sub>3</sub>O<sub>4</sub>/PGR and e) and f) NiCo<sub>2</sub>O<sub>4</sub>/PGR.

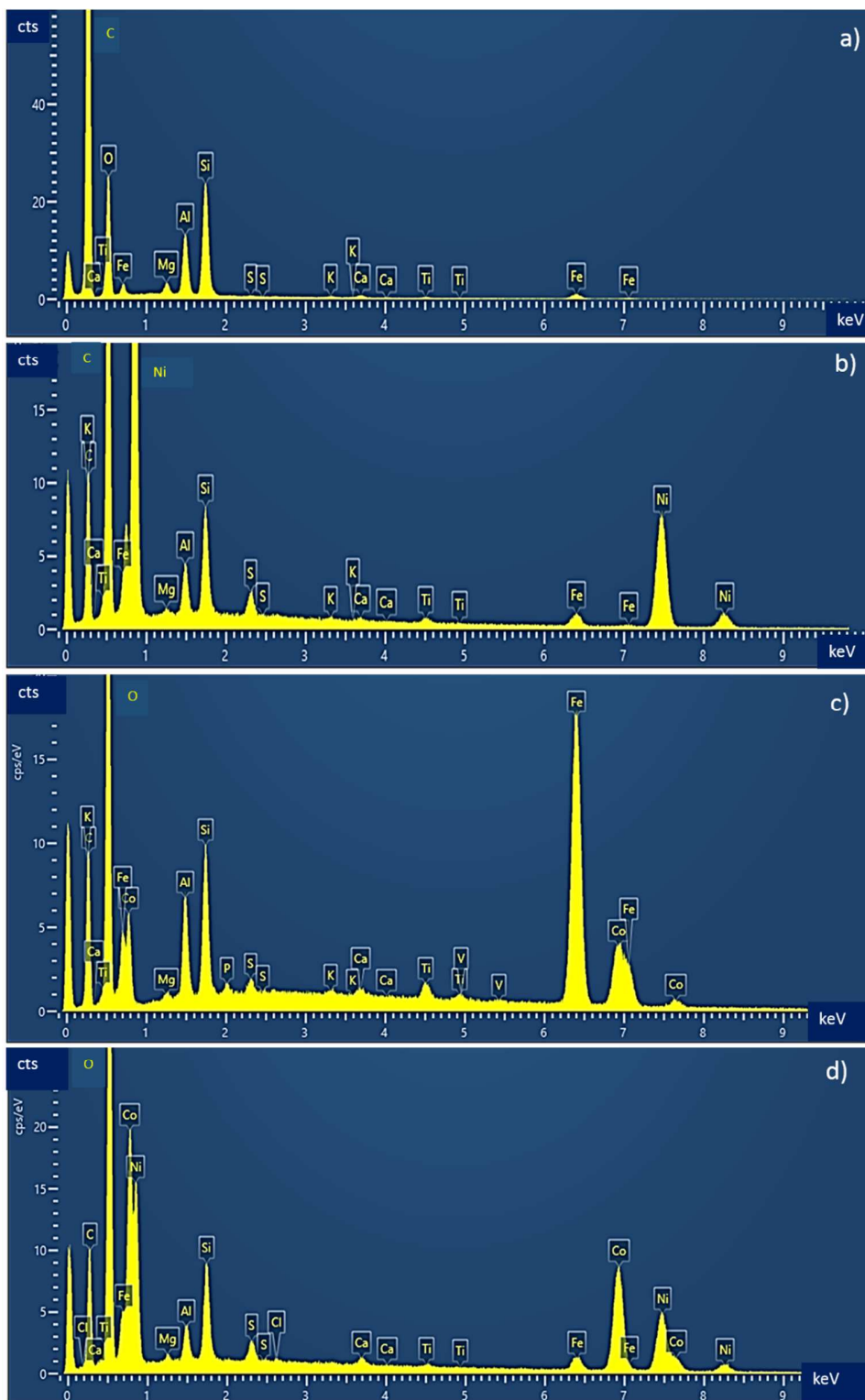


**Figure S 4:** EDS analysis of a) PGR, and the prepared electrocatalysts: b) NiO/PGR, c) Co<sub>3</sub>O<sub>4</sub>/PGR and d) NiCo<sub>2</sub>O<sub>4</sub>/PGR.

**Table S1:** Comparison of average elemental composition of GPR and the prepared electrocatalysts extracted from EDS spectra.

at. %	GPR	NiO/PGR	Co <sub>3</sub> O <sub>4</sub> /PGR	NiCo <sub>2</sub> O <sub>4</sub> /PGR	NiO/PGR	Co <sub>3</sub> O <sub>4</sub> /PGR	NiCo <sub>2</sub> O <sub>4</sub> /PGR
	Before OER experiment				After OER experiment		
<b>C</b>	76.5	19.4	35.6	32.5	12.3	22.9	24.5
<b>O</b>	17.3	22.3	41.2	38.2	44.5	49.5	19.4
<b>Na</b>	-	0.1	-	0.1	0.3	-	0.1
<b>Mg</b>	0.2	0.1	0.2	0.3	-	0.1	0.1
<b>Al</b>	1.5	1.0	0.9	1.2	1.0	0.6	0.8
<b>Si</b>	3.6	2.7	1.5	2.8	2.1	0.8	1.6
<b>S</b>	-	1.1	0.2	0.6	0.6	0.2	0.3
<b>Ca</b>	0.1	0.2	0.1	0.3	0.1	0.3	0.2
<b>Fe</b>	0.7	2.2	0.6	1.3	1.2	0.7	2.1
<b>Co</b>	-	-	19.6	13.4	-	24.9	34.1
<b>Ni</b>	-	51.0	-	9.5	37.9	-	16.8

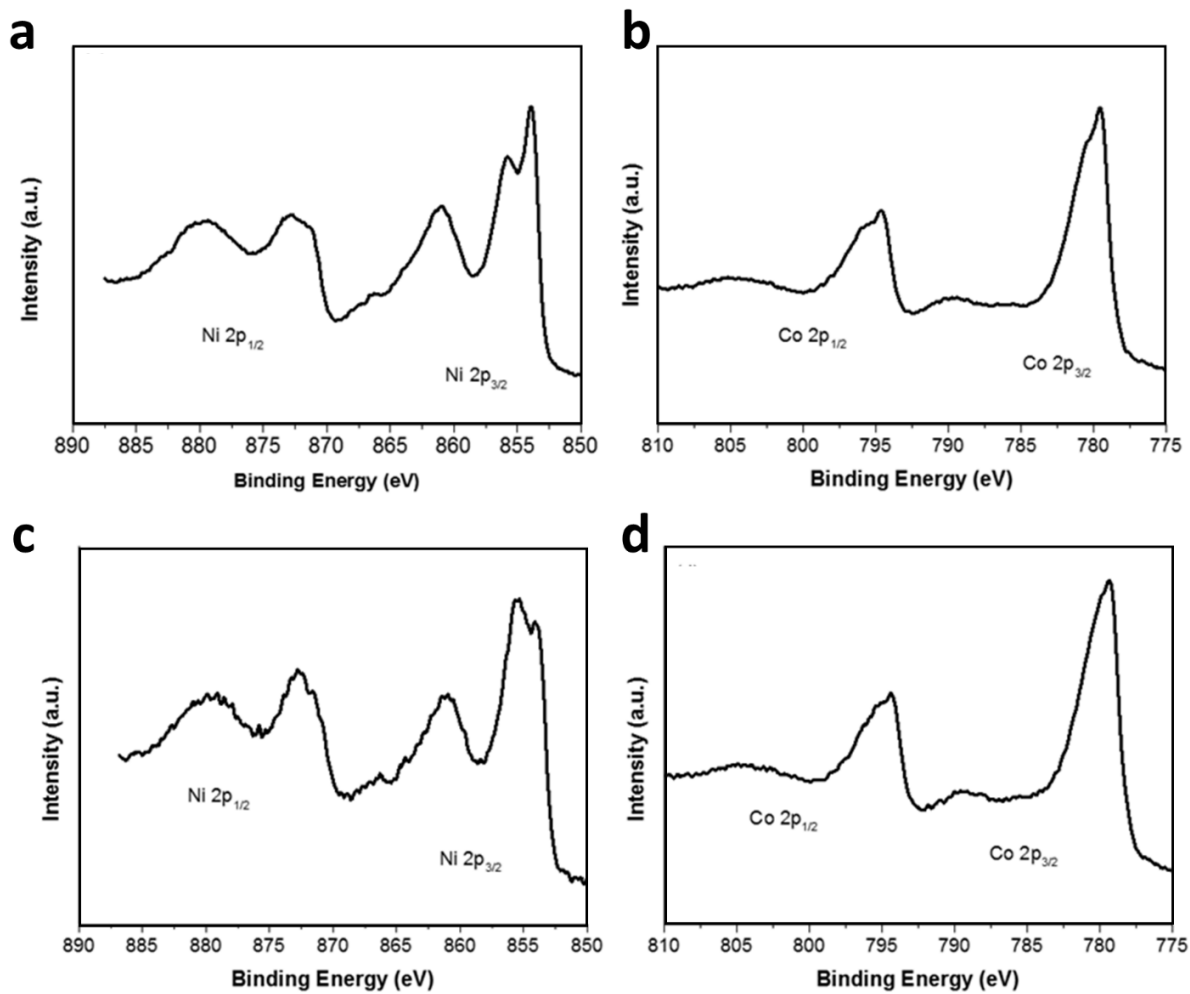


**Figure S5:** XPS spectra (a) Ni 2p of NiO/PGR; (b) Co 2p of Co<sub>3</sub>O<sub>4</sub>/PGR; (c) Ni 2p and (d) Co 2p of NiCo<sub>2</sub>O<sub>4</sub>/PGR.

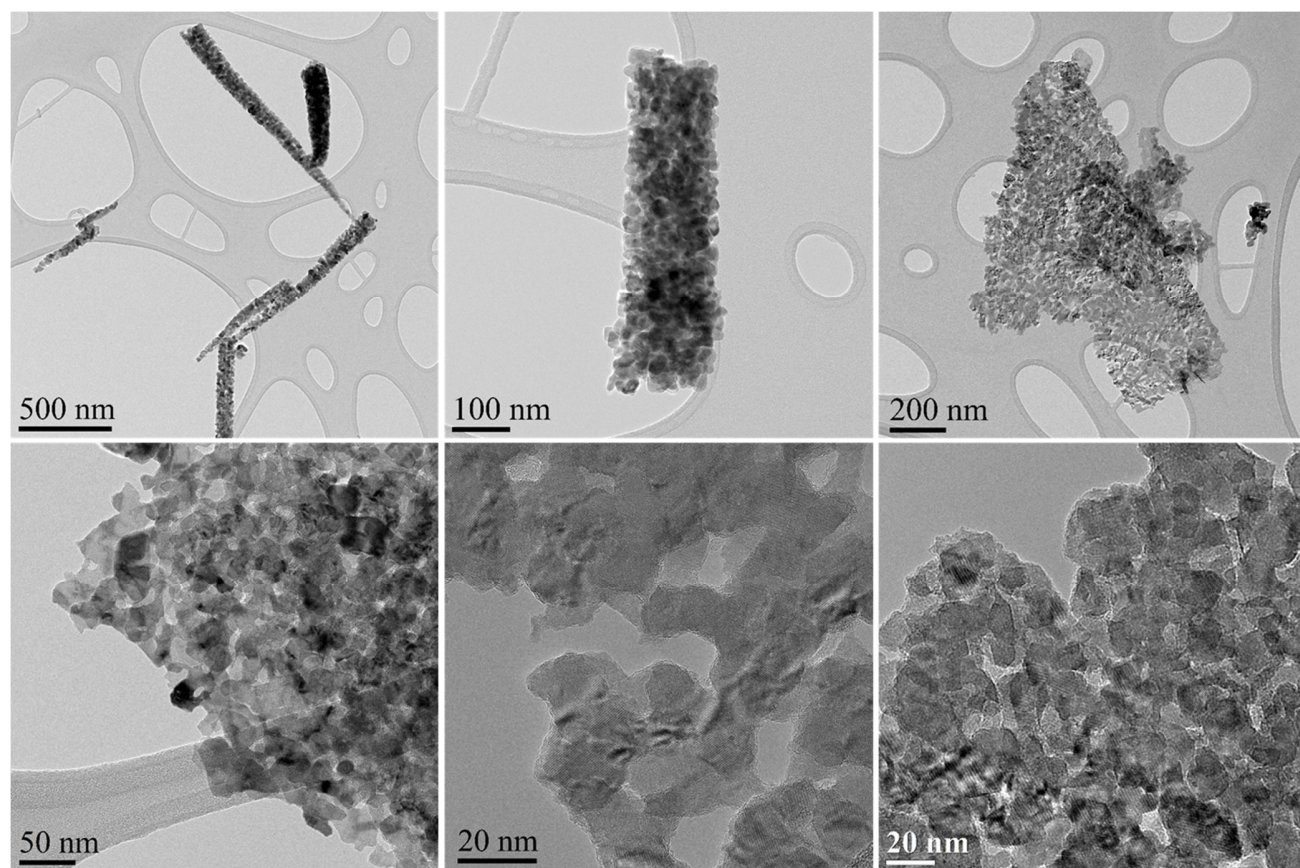


**Figure S6:** TEM images of NiCo<sub>2</sub>O<sub>4</sub>/PGR before OER experiments at different magnifications.

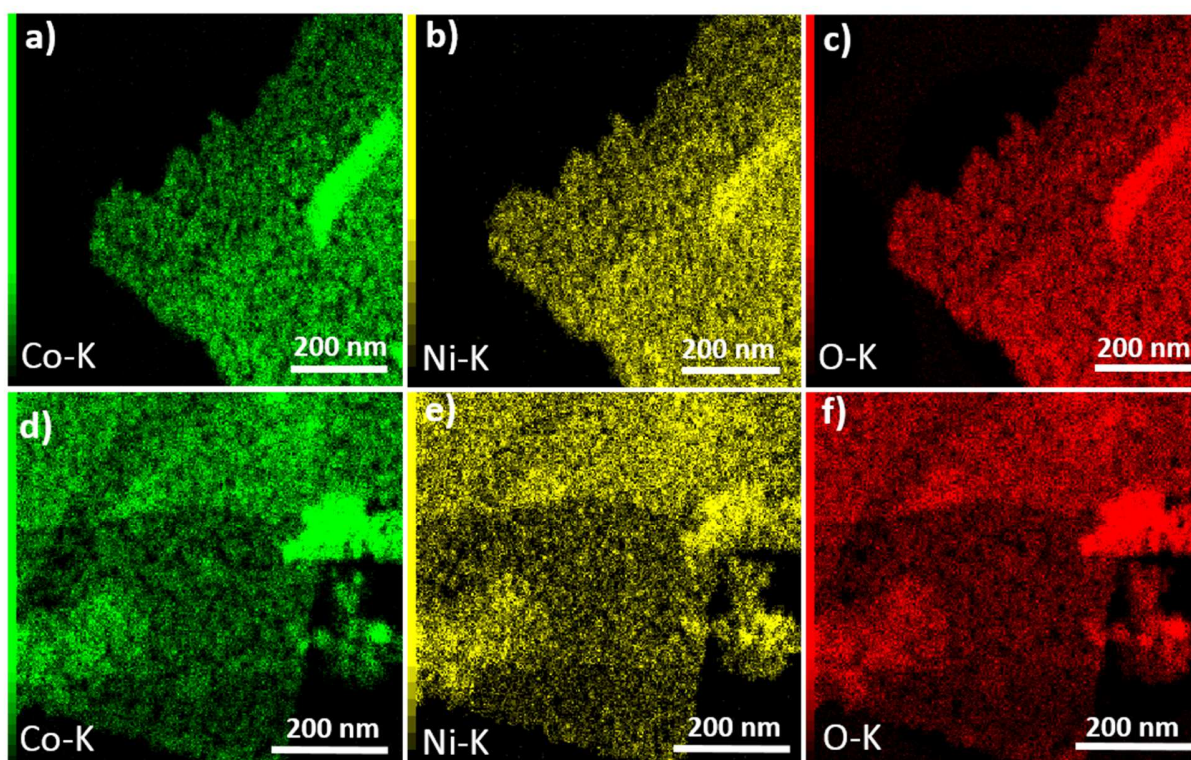


**Figure S7:** X-maps from EDS analyses of NiCo<sub>2</sub>O<sub>4</sub>/PGR before (a-c) and after (d-f) the OER reactions.

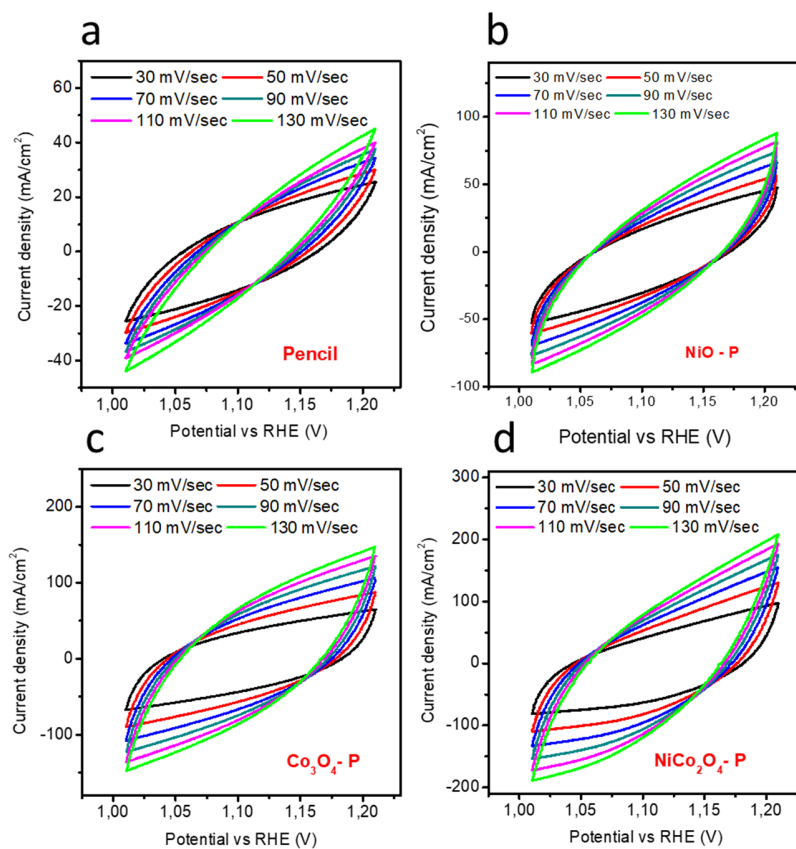


**Figure S8,** a. CV curves of bare graphite pencil at different scan rates in 1.0 M KOH, b. CV curves of NiO-P at different scan rate in 1.0 M KOH, c. CV curves of  $\text{Co}_3\text{O}_4\text{-P}$  at different scan rates in 1.0 M KOH, d. CV curves of  $\text{NiCo}_2\text{O}_4\text{-P}$  at different scan rates in 1.0 M KOH

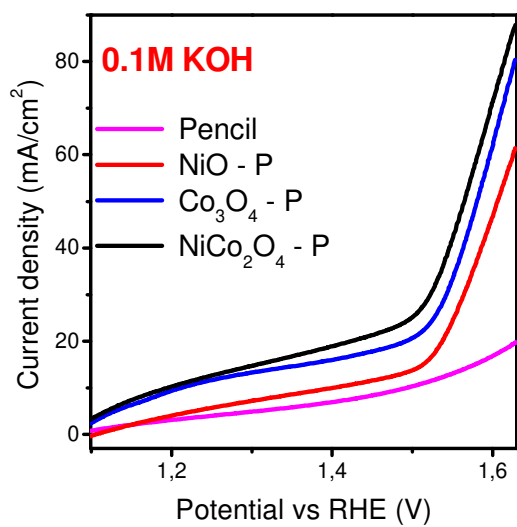


**Figure S9** . LSV curves of bare graphite pencil, NiO-P, Co<sub>3</sub>O<sub>4</sub>-P, NiCo<sub>2</sub>O<sub>4</sub>-P, at a scan rate of 5mVs<sup>-1</sup> in 0.1 M KOH